PARAMAGNETIC RESONANCE OF Mn^{+2} IONS IN NATURAL CRYSTALS OF MONTICELLITE

by

Alexander G. Danilov

Submitted in partial fulfillment
of the requirements for the degree of
Master of Science

Department of Physics,
Faculty of Pure and Applied Science,
The University of Ottawa,
Ottawa, Canada.

1968

© Alexander G. Danilov 1969

ABSTRACT

The paramagnetic resonance spectrum of Mn^{+2} impurity ions in natural crystals of monticellite, $MgCaSiO_4$, was studied at room temperature and at x and q-band microwave frequencies. Four magnetic complexes, which in the (010) plane degenerate into two, were discovered. The magnetic field separation of the spectral lines along the principal axes of the crystalline electric field was the same for all four complexes. Partial angular variation of spectral splitting was done in this plane and confirmed the existence of two complexes closely related in pairs. The spectrum was fitted to a spin Hamiltonian for S state ions in crystalline electric field of orthorhombic symmetry. The spin Hamiltonian, including hyperfine structure, is given by

$$= \beta g_x S_x H_x + \beta g_y S_y H_y + \beta g_z S_z H_z$$

$$+ \frac{1}{3} b_2^0 O_2^0 + \frac{1}{3} b_2^2 O_2^2 + \frac{1}{60} b_4^0 O_4^0 + \frac{1}{60} b_4^2 O_4^2 + \frac{1}{60} b_4^4 O_4^4$$

$$+ A I_z S_z + B I_y S_y + C I_x S_x .$$

The parameters were determined as:

$g_z = 1.9961 \pm .0010$, $g_y = 1.9905 \pm .0010$, $b_2^0 = -558.5$, $b_2^2 = -351.7$, $b_4^0 = -0.5$, $b_4^2 = -56.0$, $b_4^4 = -40.3$, $A = 85.5$, $B = 85.5$. The values of b_n^m, A and B, are in gauss and the signs are relative. These parameters were used to diagonalize the matrix of the spin Hamiltonian for incremental values of magnetic field along a Z axis. On the basis of this, an energy level diagram as a function of externally applied magnetic field was obtained.

It was possible to relate the Mn^{+2} spectra to the crystal struc-

ture of monticellite. In particular it was shown that Mn^{+2} impurity ions replace Mg atoms which are in centers of symmetry and do not replace Ca ions which are in sites of lower symmetry. Indications were found which suggest that the crystal structure of monticellite should be redetermined if precise positions of atoms in the unit cell are required.

ACKNOWLEDGEMENTS

The author wishes to thank Dr. A. Manoogian for suggestion of the problem and for guidance during the course of the research. His constant interest and encouragement is greatly appreciated. Thanks are also due to Mr. B.W. Chan for his dexterous operation of the spectrometers and to Mr. N. Goodchild and his shop staff for construction of microwave cavities. Financial assistance from Dr. A. Manoogian's National Research Council grant and an Ontario Government Graduate Fellowship is gratefully acknowledged. Finally, the author wishes to thank his wife, Raisa, for typing the manuscript.

LIST OF ILLUSTRATIONS

LIST OF TABLES

TABLE OF CONTENTS

CHAPTER I

INTRODUCTION

The phenomenon of electron spin resonance (ESR), since its discovery about twenty five years ago, has proved to be very useful as a research and analytic tool in quite diverse fields. In particular the technique has been used to study the ground state of paramagnetic impurity ions in crystals, and the effect on the ground state due to the electrostatic environment that the paramagnetic ion experiences. The study of this effect can often tell much about the host crystal itself, and it is with this question that the present investigation is mainly concerned. The research involves studying the paramagnetic resonance spectra of Mn^{+2} impurities in natural crystals of monticellite, $CaMgSiO_4$.

It is well known that paramagnetic ions in crystalline environment experience a partial removal of energy state degeneracy due to electrostatic interaction with the nearest neighbours in the lattice. In this connection the S state ions are of particular interest in that due to their spherical electron distribution all the spin states would have equal interaction energies with an electrostatic environment and hence no removal of degeneracy would be expected. The fact is that Mn^{+2}, which is an S state ion with ground state electron configuration $1s^2 2s^2 2p^6 3s^2 3p^6 3d^5$ and term $^6S_{5/2}$, does experience a crystal splitting of its ground state.

Mechanisms to explain this effect have been proposed. Van Vleck

and Penney[1] have shown that a small admixture to the $^6S_{5/2}$ state of higher multiplets and configurations (e.g. $4s^2$) can cause crystal field splitting, commonly known as zero field splitting, through higher order interactions. There would be no first order effects either in the crystal field splitting or in the spin orbit coupling. Another mechanism is offered by Abragam and Pryce[2] who discuss a second order effect due to spin-spin interactions of the five 3d electron cloud distribution and hence allow the crystalline field to separate levels due to different Ms values.

It has been shown by Gabriel et al[3], however, that configurational mixing is not quantitatively sufficient to account for the observed zero field splitting of these ions. Ayscough[4] claims that calculations which consider the polarization effect of the lower lying 2s and 3s electrons in Mn^{+2} by the net spin of the $3d^5$ electrons give good agreement with experiment.

It is seen that in spite of the mechanisms proposed to explain the zero field splitting some doubt remains as to whether these provide the complete explanation. Although the theoretical aspects of S state zero field splitting are somewhat unresolved the experimental observation of these splittings through their effect on the paramagnetic absorption spectra yield often important information about the host.

Recently, the fields of mineralogy and geology have adopted the ESR technique as an analytic tool. Here of course, the interest is not restricted to S states only but includes all paramagnetic ions. This is not surprising when one notes that a large number of paramagnetic ions are available. These include: the first transition group ($3d^n$), the palladium group ($4d^n$), the platinum group ($5d^n$), the rare earth group ($4f^n$), and the actinides group $(5f^n)^5$.

Some advantages offered by the method of ESR analysis are considerable. It is possible often to detect minute quantities of an impurity, 10^{-12} gramme in some cases[5]. Also one may be able to determine whether the occupation of the host is substitutional or interstitial. Type of bonding can be predicted through the study of hyperfine structure.

In the present work one member of a group of minerals has been studied, i.e., monticellite, which belongs to the olivine group. The paramagnetic impurity in monticellite has been identified and through the study of the spectrum it is possible to state unambiguously which of the available cation sites is occupied, and that it is substitutional in character. It is demonstrated that a crystal structure redetermination is warranted if precise positions of atoms in the unit cell are required. The word precise is meant to include differences of .1 angstrom.

The resonance study of monticellite was done at X-band (9.4 GHz) and q-band (35 GHz) microwave frequencies, with most of the final results being obtained at q-band. All measurements were performed at room temperature. Low temperature ($4.2^{o}K$) spectra were also obtained, but the resonance lines were poorly resolved and so they could not be used. The spectral lines obtained at q-band were fitted to a spin Hamiltonian of orthorhombic symmetry, as done by Vinokurov et al[6] in their study of Mn^{+2} in diopside crystal.

The results obtained for Mn^{+2} in monticellite are compared with those obtained for Fe^{+3} in chrysoberyl by Vinokurov et al[7]. This is of some interest because both minerals belong to the same space group. Also there has been a redetermination of crystal structure of chrysoberyl subsequent to the ESR study by Vinokurov et al. And this

refined structure is not in such good agreement with the ESR results as reported. Because of structural similarity to monticellite one is tempted to expect analogy in ESR results also. This possibility is examined in the conclusion.

CHAPTER II

CRYSTALLOGRAPHY

Monticellite is a member of the olivine group of orthorhombic orthosilicates. The chemical formula for the group is R_2SiO_4. R may be Mg, Fe, or Mn. Members of the group and their cell dimensions are given in Table I[8].

TABLE I Olivine Group

Mineral	Formula	a (Å)	b (Å)	c (Å)
Forsterite	Mg_2SiO_4	4.76	10.21	5.98
Fayalite	Fe_2SiO_4	4.80	10.59	6.16
Tephroite	Mn_2SiO_4	4.87	10.64	6.23
Monticellite	$CaMgSiO_4$	4.82	11.08	6.37

The name olivine is given to solid solutions of forsterite and fayalite, i.e. $(MgFe)_2SiO_4$. Fayalite and tephroite may also form solid solutions of varying composition, i.e. $(Fe,Mn)_2SiO_4$, which is known as knebelite. Monticellite, along with other members of the olivine family, have the space group $P_{nma}(D_{2h}^{16})$. The notation in brackets is due to Schoenflies, whereas the other is the international notation of 1952. D stands for dihedral group and 2h for a two-fold

rotation axis combined with a horizontal plane perpendicular to the rotation axis. The index 16 means that it is the sixteenth available space group consistent with the orthorhombic symmetry as listed in conventional tables. In the International notation P stands for primitive cell. The subscript n defines a glide operation: a translation $(\frac{b}{2} + \frac{c}{2})$ followed by a reflection in the (100) plane. The subscript m stands for a mirror plane parallel to the (010) plane. The subscript a also defines a glide plane with translation $\frac{a}{2}$ followed by a reflection in the (001) plane. Thus it is seen that P_{nma} is a holohedral orthorhombic space group since there are three sets of reflection planes.

There are four chemical units in the unit cell. The ionic charges are: $Mg^{+2}Ca^{+2}(SiO_4)^{-4}$. Thus the available cation sites for substitution by Mn^{+2} in monticellite are those of Mg^{+2} and Ca^{+2}. Table 2 gives some properties of ions in monticellite.

TABLE 2 Characteristics Of Ions In Monticellite

Atom	Atomic Number	Ion Formed	Number of Electrons in Ion	Ground Config. of Ion	Ionic Rad. o In A
Mg	12	Mg^{+2}	10	$1s^2 2s^2 2p^6$	0.65
Ca	20	Ca^{+2}	18	$(A)^{18}$*	0.99
Si	14	Si^{+4}	10	$1s^2 2s^2 2p^6$	0.41
O	8	O^{-2}	10	$1s^2 2s^2 2p^6$	1.40
Mn	25	Mn^{+2}	23	$(A)^{18} 3d^5$	0.80

* $(A)^{18}$ stands for the argon core: $1s^2 2s^2 2p^6 3s^2 3p^6$.

The structure of monticellite was determined by Brown and West[9] more than forty years ago. Its essential features were determined as follows: (a) oxygen atoms form two sheets parallel to (100); (b) the oxygen positions show approximate hexagonal close packing; (c) the silicon atoms are at centers of tetrahedra formed by four oxygens; (d) every magnesium and calcium atom is surrounded nearly octahedrally by six oxygen atoms; (e) the magnesium octahedral sites are centers of symmetry whereas the calcium octahedral sites are located on reflections planes; (f) there are three types of oxygen atoms; (g) the silicon-oxygen tetrahedra point alternately in opposite directions along both the a and b directions in accordance with the holohedral symmetry. The location of atoms in the unit cell after Brown and West is given in Table 3. The structure of monticellite, based on data from Table 3, is shown projected on (100) in Figure 1.

TABLE 3 Coordinates Of Atoms In Unit Cell Of Monticellite[9]

Kind of Atom	No. of Atoms in Unit Cell	x (Å)	y (Å)	z (Å)
Mg	4	0.0	0.0	0.0
Ca	4	-.082	2.848	1.593
Si	4	1.940	.953	1.593
O_1	4	-1.136	.742	1.593
O_2	4	1.271	4.809	1.593
O_3	8	1.204	1.695	.191

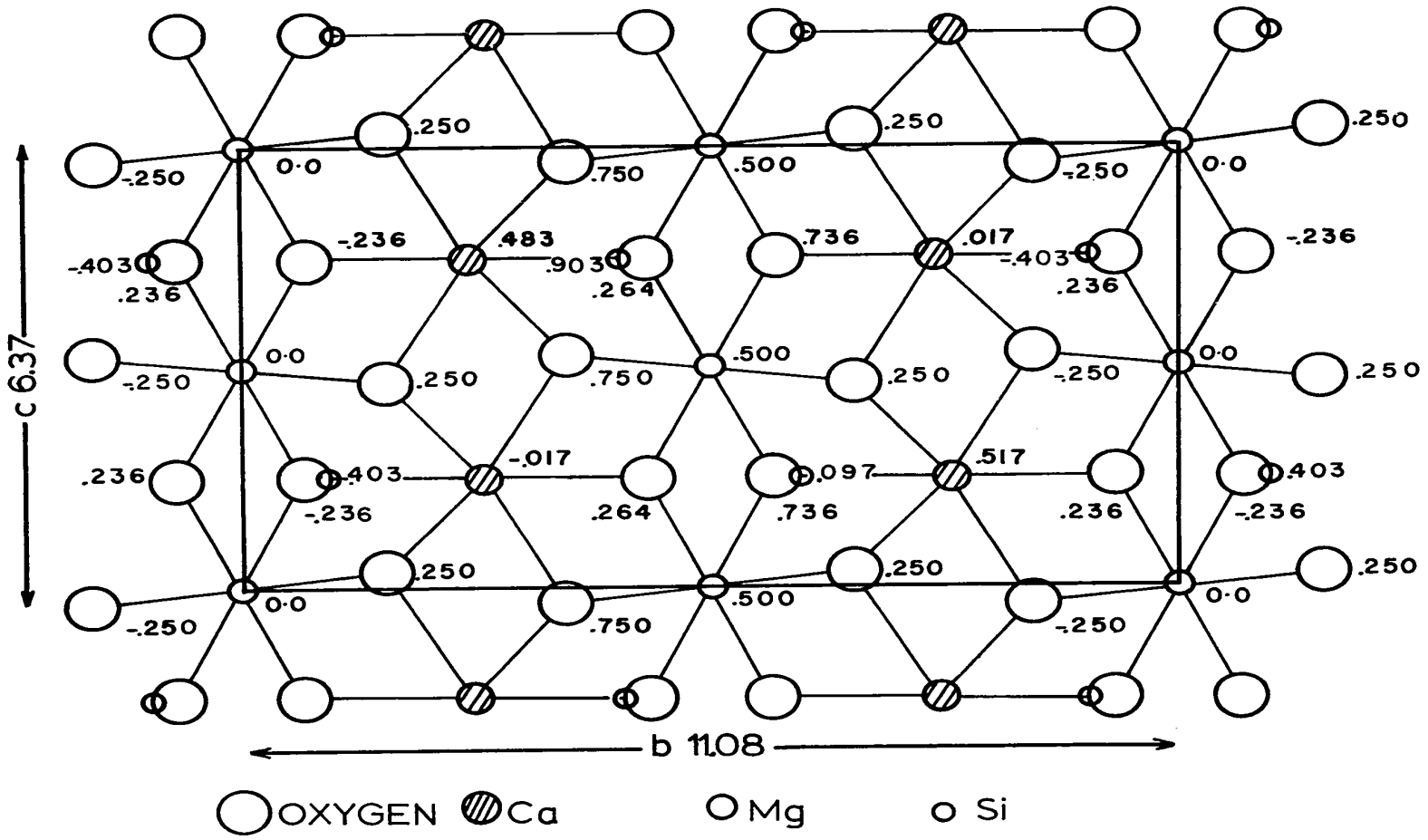

Fig. 1. Unit cell of monticellite projected on (100). Bonds mark out oxygen octahedra for magnesium and calcium sites. The structure is based on data by Brown and West[9]. Decimal fractions give distance of atoms above or below paper plane.

There does not seem to be any recent structure determination of monticellite. However, Bragg and Claringbull[8] give details for a recent determination of the structure of forsterite, Mg_2SiO_4. Monticellite is said to resemble forsterite very closely with half the magnesium atoms of forsterite being replaced by calcium atoms. Figure 2 gives the structure of forsterite projected on (100), according to Bragg and Claringbull with half the magnesium ions replaced by calcium ions. The sites designated α, $\bar{\alpha}$, β, $\bar{\beta}$, γ, $\bar{\gamma}$, δ, $\bar{\delta}$ in Figure 2 consist of Ca and Mg atoms surrounded by nearly regular octahedrons of oxygen atoms. These sites are shown projected on (010) in Figure 3. In Figure 3(a) and (b) it can be seen that the four sites α, $\bar{\alpha}$, β, $\bar{\beta}$, which are occupied by magnesium atoms, are crystallographically identical. These sites have centers of symmetry (inversion centers) and also two-fold rotation axes parallel to [010]. Figure 3(c) and (d) shows the calcium sites denoted by γ, $\bar{\gamma}$, δ, $\bar{\delta}$ in Figure 2. These sites are also crystallographically identical but the only symmetry element they possess is a mirror plane (001).

The chief difference between the structure determination of monticellite given by Brown and West and of that indicated by Bragg and Claringbull is that the oxygen atoms surrounding the Ca and Mg atoms are more symmetrically arranged in the former case. For example, in Figure 3(a) the angles between the C axis and two oxygen projections are 34° and 41° according to Bragg and Claringbull; but these angles would be identical, and equal to about 36°, according to Brown and West.

The specimen of monticellite on which most of the ESR work was done, had dimensions of about 2mm x 2mm x 3mm. The single crystal nature of the specimen was determined by X-ray measurements, employing the precession camera technique. The facilities of the Department of

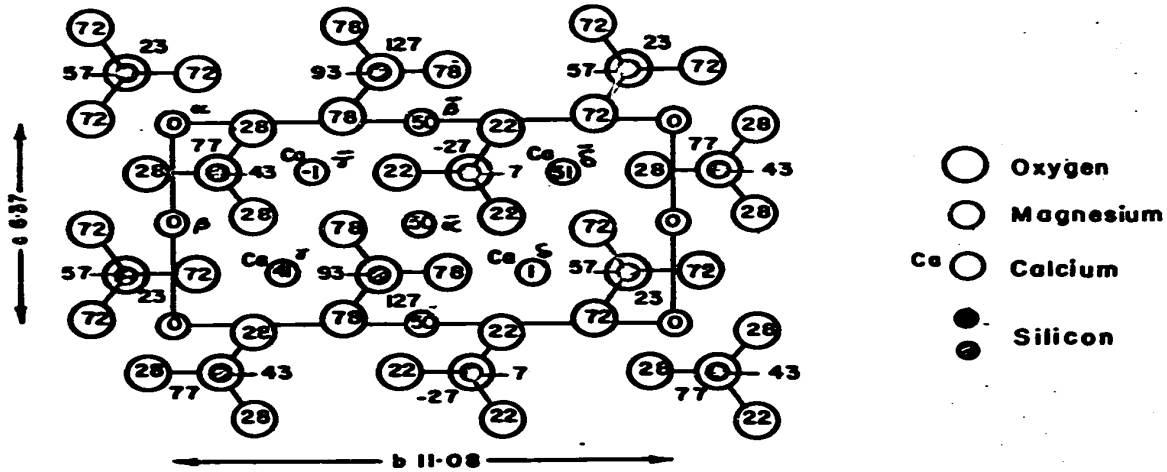

Fig. 2. Unit cell of monticellite projected on (100). Bonds mark out SiO_4 tetrahedra. This structure is as given by Bragg and Claringbull[8] for forsterite with half the Mg^{+2} ions replaced by Ca^{+2} ions as indicated. Magnesium sites are designated α, $\bar{\alpha}$, β, and $\bar{\beta}$, calcium sites γ, $\bar{\gamma}$, δ, and $\bar{\delta}$. Numbers give, in per cent of unit cell, distance of atoms above or below paper plane.

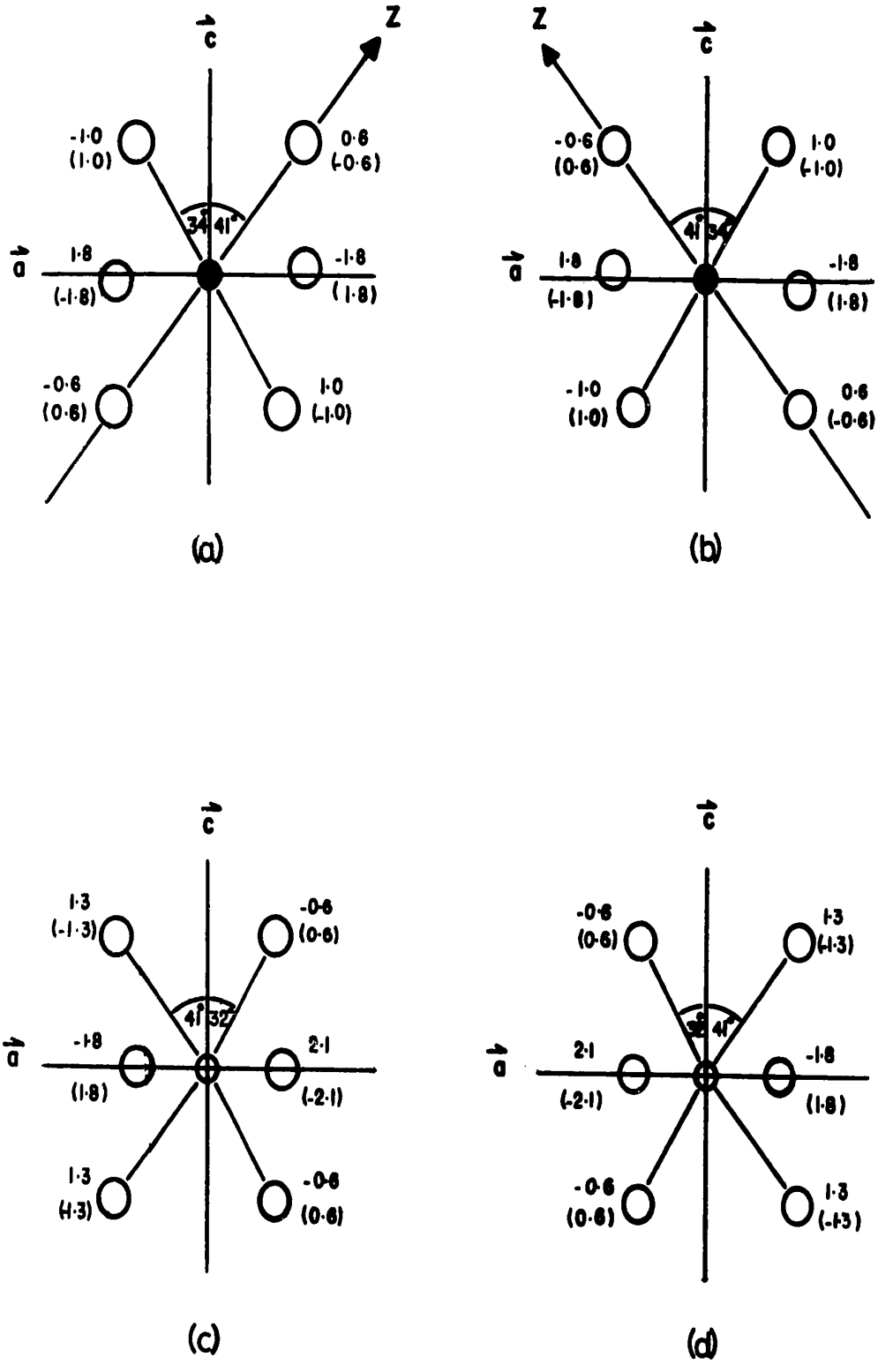

Fig. 3. Magnesium sites (a) and (b), calcium sites (c) and (d), projected on (010). α, $\bar{\alpha}$ sites are shown in (a), β, $\bar{\beta}$ in (b), γ, $\bar{\gamma}$ in (c), δ, $\bar{\delta}$ in (d). The scale is 1/4" = 1A, and in each case the elevation in parenthesis refers to barred sites.

Energy, Mines and Resources, Ottawa, were used in this case. This method also allowed the determination of the crystal parameters. The crystal orientation and the two unit cell dimensions were confirmed employing the back reflection Laue and the rotating-crystal methods. This work was done using a Philips goniometer. The specimen, mounted on a perspex pin, when attached to the goniometer could be rotated in a vertical plane, giving an angle θ, and in the horizontal plane giving an angle ϕ. The X-radiation was in a horizontal direction.

Back reflection Laue photographs were obtained for two orientations 90° apart. Both exhibited orthogonal planes of symmetry. One of these photographs is shown in Figure 4 (a). The incident white radiation (from a copper target) was normal to the films and was thus parallel to important directions in the crystal. The angular coordinates θ and ϕ for these directions were plotted on a stereogram. Using the rotating-crystal method, these directions were found to be coincident with the $\vec{c}$ and $\vec{b}$ axes. The third axis, $\vec{a}$ was plotted normal to $\vec{b}$ and $\vec{c}$. This is shown on the stereogram in Figure 9, which also shows the position of magnetic axes for the two complexes of Mn^{+2}.

In the rotating-crystal method the sample is slowly rotated about a direction parallel to a zone axis and monochromatic radiation is incident normal to this direction. Figure 4 (b) shows a photograph obtained for one of the two orientations given above. When the zone axes correspond to crystallographic axes, as was the case for the above orientations, crystal parameters may be calculated from the formula,

$$\text{parameter} = n\lambda / \text{Cos}(\omega)$$

where, $n = 1, 2, - -$ is the order of diffraction, λ is the radiation wavelength, and $\text{Tan}(\omega) = D/r$, where D is the specimen-to-film distance and r is the distance between the $n = 0$ and $n = n$ lines. The unit cell

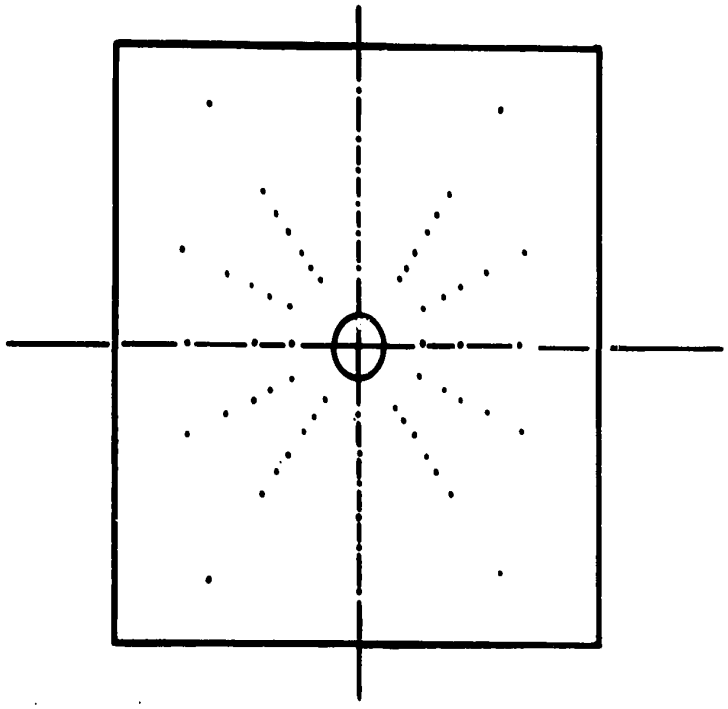

(a)

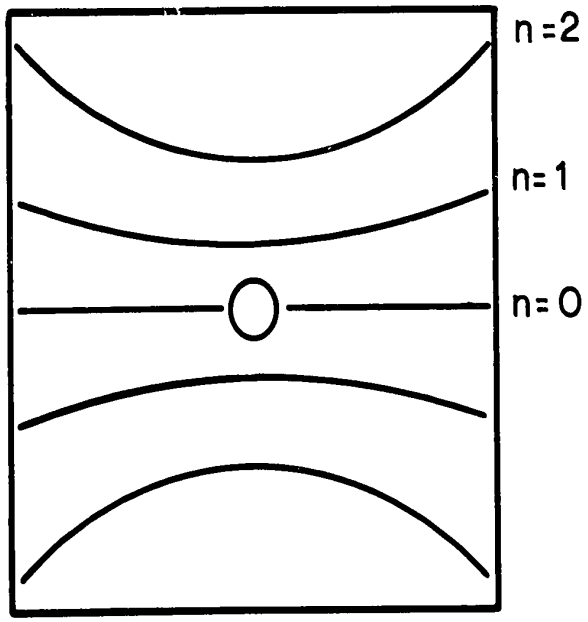

(b)

Fig. 4. (a) Shows a typical back reflection Laue photograph obtained for x radiation parallel to a crystallographic axis. (b) Shows a back reflection photograph for a slowly rotated specimen. In this case radiation was normal to $\vec{b}$ axis.

dimensions along $\vec{b}$ and $\vec{c}$ obtained with this method are given in Table 4.

TABLE 4 Comparison Of Calculated Parameters With Accepted Values For Monticellite

Rotation Parallel to	Calculated Parameter	Accepted Value
b axis	11.06 Å	11.08 Å
c axis	6.18 Å	6.37 Å

CHAPTER III

T H E O R Y

A. Introduction

The important terms in the general Hamiltonian of an ion in a crystalline environment and subjected to an external magnetic field H can be written as[6]

$$\mathcal{H} = \mathcal{H}_{1} + \mathcal{H}_{[illegible]} + \mathcal{H}_{[illegible]} + \mathcal{H}_{[illegible]} + \mathcal{H}_{[illegible]} + \mathcal{H}_{[illegible]} + \mathcal{H}_{[illegible]}$$

[illegible] of the terms are as follows:

[illegible] term $\mathcal{H}_1$ represents the total kinetic energy of the [illegible] attraction between the electrons and the nucleus, [illegible] between the individual electrons. It is written as

[illegible]

[illegible] mass m and charge e, [illegible] with respect to [illegible]

[illegible]

[illegible] term gives [illegible] to [illegible]

ESR studies it is only the lowest energy level that is of interest since this is the one that is appreciably populated.

(ii) $\mathcal{H}_{LS}$ gives the energy due to spin-orbit coupling, and may be written as

$$\mathcal{H}_{LS} = \sum_{I,J} \lambda_{I,J} \vec{l}_I \cdot \vec{s}_J$$

where $\vec{l}_I$ is the orbital angular momentum of the Ith electron,

$\vec{s}_J$ is the spin angular momentum of the Jth electron, and

$\lambda_{I,J}$ is an interaction constant and the summation is over all the electrons in the atom.

If one considers energy states derived from the ground state (given by $\mathcal{H}_E$) the spin orbit interaction may be written more simply as

$$\mathcal{H}_{LS} = \lambda \vec{L} \cdot \vec{S}$$

where $\vec{L}$ is the free ion orbital angular momentum, and

$\vec{S}$ is the free ion spin angular momentum.

The magnitude of this effect varies with the strength of the coupling and the ion state but it is generally between 10^2 and 10^3 cm^{-1}.

(iii) The nuclotic interaction between each electron and the nucleus is given by

$$\mathcal{H}_{SI} = \sum_I \vec{s}_I \cdot \vec{j}_I \cdot \vec{I}_I$$

where $\vec{j}_I$ is the total angular momentum of the Ith electron,

$\vec{I}_I$ is the nuclear spin and

$\vec{s}_I$ is the coupling factor for the interaction.

this interaction produces the hyperfine levels which are of the order of 10^{-2} cm^{-1} in separation.

(iv) $^{3}P_{1}$ describes a very small effect. It is of the order of 10^{-4} cm^{-1} and is attributed to the nuclear quadrupole interaction which is to effect the nuclei with spin greater than $\frac{1}{2}$. Its effect can be neglected in this work because the selection rule for ΔF causes the term to vanish for allowed transitions.

(v) The expression for the effect due to the applied field is

$$\Delta E = \mu_B g_J M_J H$$

where μ_B is the Bohr magneton, g_J is the Landé g factor, M_J is the magnetic quantum number, and H is the applied field.

C. Hyperfine Structure

The interaction energy producing the hyperfine splitting can arise in two ways. First there is the dipolar interaction of magnetic moments of the nuclear and electron spin. This interaction is anisotropic since it depends on the direction joining the electron and nucleus. The spherically symmetric electron distribution of the $3d^5$ electrons in Mn^{+2} [illegible] spin density at the nucleus. Hence there should be no hyperfine splitting due to this interaction for S-state ions.

The other source of hyperfine splitting is attributed to the so-called Fermi contact interaction which is isotropic. The contact [illegible] finite unpaired spin density at the nucleus due to S-[illegible] to configurational mixture of orbitals. In [illegible] the ground state instead of being a simple $3s^2\ 3d^5$ [illegible] nature of the $3s^1\ 3d^5\ 4s^1$ and the $3s^2\ 3d^5$ [illegible]

[illegible]

[illegible] electrons,

[illegible] the contact term quantizes [illegible] different orientations causing [illegible] the stem and splitting each [illegible] lines, $I = 5/2$ [illegible] unequally spaced.

The spacing can be predicted from perturbation theory which involves the second order approximation.

D. The Spin Hamiltonian

The Hamiltonian for a paramagnetic ion in a crystalline electric field is in general quite complicated. Pryce[12] and Abragam and Pryce[2] have developed a very useful method for carrying out the perturbation calculation, and have applied it especially to the iron group. This calculation is based on the fact that transitions between the lowest energy levels are observed in the phenomenon of paramagnetic resonance. If transitions between $2S'+1$ levels are observed experimentally, then S' can be defined as the fictitious spin of the system. In some cases, e.g. in the $^6S_{5/2}$ state, the fictitious spin is identical to the free ion spin. Abragam and Pryce transform the various terms in the Hamiltonian into a form involving appropriate angular momentum operators L,S and J. The advantage of using a spin Hamiltonian is that the rather complicated behaviour of the lowest energy levels of the paramagnetic ion in a magnetic field can be described in a relatively simple way by specifying the effective spin, together with a small number of parameters which measure the magnitudes of the various terms in the Hamiltonian. One must then find a model of a crystal field which corresponds to the spin Hamiltonian and which will explain the observed parameters.

The interaction terms describing the paramagnetic resonance spectrum of a Mn^{+2} ion in the spin Hamiltonian are as follows:

(1) Zeeman term. The Zeeman term can be written for the case of an orbital singlet with tensor g value as

$$\mathcal{H}_{SH} = \beta S \cdot g \cdot H$$

$$= \beta g_x S_x H_x + \beta g_y S_y H_y + \beta g_z S_z H_z$$

(ii) Hyperfine term. Following Abragam and Pryce[2], the hyperfine interaction given by the contact term discussed above can be written as

$$\mathcal{H}_{SI} = \sum_{i,j} A_{ij} I_i S_j$$

where $i,j = x,y,z$,

A_{ij} is the hyperfine coupling tensor,

I is the nuclear spin, and

S is the total electron spin.

The principal axes of A_{ij} are taken to be along the g tensor axes. Hence, for an orthorhombic crystalline electric field we can write

$$\mathcal{H}_{SI} = A I_z S_z + B I_y S_y + C I_x S_x$$

(iii) Crystalline electric field interaction. The spin Hamiltonian for a crystalline electric field of orthorhombic symmetry is given by Vinokurov et al[6] as being

$$\mathcal{H}_{CF} = \frac{1}{3} b_2^0 O_2^0 + \frac{1}{3} b_2^2 O_2^2 + \frac{1}{60} b_4^0 O_4^0 + \frac{1}{60} b_4^2 O_4^2 + \frac{1}{60} b_4^4 O_4^4 .$$

The form of these operators are given by Orbach[13]:

$$O_2^0 = 3S_z^2 - S(S+1)$$

$$O_2^2 = \frac{1}{2}(S_+^2 + S_-^2)$$

$$O_4^0 = 35S_z^2 - [30S(S+1) - 25] S_z^2 - 6S(S+1) + 3S^2 (S+1)^2$$

$$O_4^2 = \frac{1}{4}\left[[7S_z^2 - S(S+1) - 5] (S_+^2 + S_-^2) + (S_+^2 + S_-^2) [7S_z^2 - S(S+1) - 5] \right]$$

$$O_4^4 = \frac{1}{2}(S_+^4 + S_-^4)$$

where,

$$S_+ = S_x + iS_y$$

$$S_- = S_x - iS_y.$$

The matrix elements for these operators in various manifolds are given by Stevens[14], and by Jones, Baker and Pope[15], and by Low[16].
The matrix elements of O_2^0 and O_4^0 are diagonal while those of O_2^2, O_4^2 and O_4^4 are off-diagonal. Their values in the S = 5/2 manifold are:

O_2^0:

$$(\pm 1/2 \,|\, O_2^0 \,|\, \pm 1/2) = -8$$

$$(\pm 3/2 \,|\, O_2^0 \,|\, \pm 3/2) = -2$$

$$(\pm 5/2 \,|\, O_2^0 \,|\, \pm 5/2) = 10$$

O_2^2:

$$(\pm 3/2 \,|\, O_2^2 \,|\, \mp 1/2) = 3\sqrt{2}$$

$$(\pm 5/2 \,|\, O_2^2 \,|\, \pm 1/2) = \sqrt{10}$$

O_4^0:

$$(\pm 1/2 \,|\, O_4^0 \,|\, \pm 1/2) = 120$$

$$(\pm 3/2 \,|\, O_4^0 \,|\, \pm 3/2) = -180$$

$$(\pm 5/2 \,|\, O_4^0 \,|\, \pm 5/2) = 60$$

O_4^2:

$$(\pm 3/2 \,|\, O_4^2 \,|\, \mp 1/2) = -15\sqrt{2}$$

$$(\pm 5/2 \,|\, O_4^2 \,|\, \pm 1/2) = 9\sqrt{10}$$

O_4^4:

$$(\pm 5/2 \,|\, O_4^4 \,|\, \mp 3/2) = 12\sqrt{5}$$

[illegible] crystal field and hyper- [illegible]

$$\mathcal{H} = [illegible] + \frac{1}{60} B_4^0 O_4^0 + \frac{1}{60} B_4^2 O_4^2 + \frac{1}{60} B_4^4 O_4^4$$

[illegible]

The Zeeman and crystal field terms of this Hamiltonian form a (2S+1) x (2S+1) = 6x6 matrix in the S = 5/2 manifold. This matrix can be reduced to two 3x3 matrices as shown in table 5 for $H = H_z$ and $H_x = H_y = 0$.

TABLE 5 Matrix for the Spin Hamiltonian Including Zeeman And Crystal Field Terms for the Magnetic Field Along the z Direction

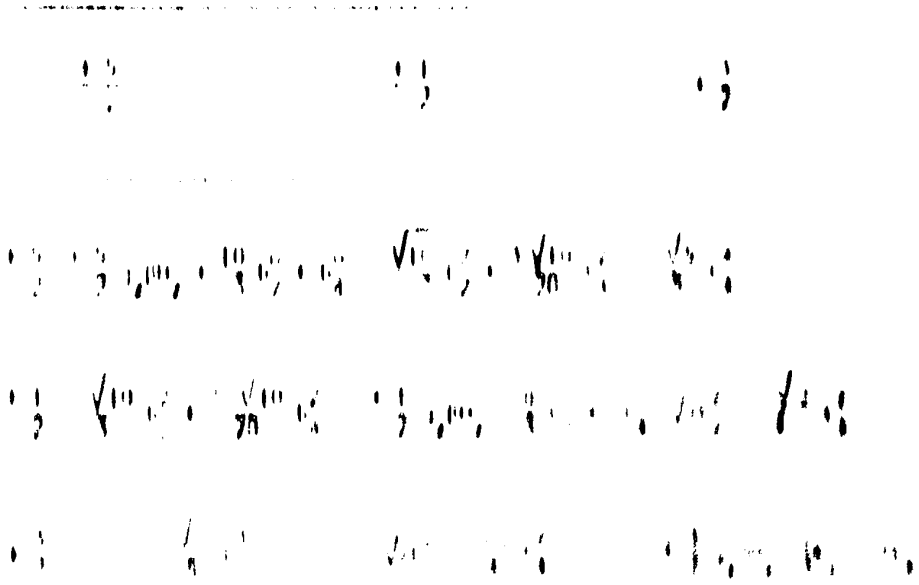

$$(\pm 5/2,m\,|\,H_{5,1}\,|\pm 3/2,m) = H_o \mp 4b_2^o \mp 4b_4^o + \frac{4}{9}\frac{(b_2^2)^2}{H_o} - \frac{1}{20}\frac{(b_4^2)^2}{H_o} - \frac{b_2^2 b_4^2}{H_o}$$

$$- Am - \frac{B^2+C^2}{4H_o}\left[\,I(I+1) - m^2\,\right] \mp \frac{2BC}{H_o}\,m. \qquad (1)$$

$$(\pm 1/2,m\,|\,H_{4,1}\,|\pm 1/2,m) = H_o \mp 2b_2^o \pm 6b_4^o - \frac{5}{9}\frac{(b_2^2)^2}{H_o} - \frac{9}{80}\frac{(b_4^2)^2}{H_o}$$

$$- \frac{1}{20}\frac{(b_4^1)^2}{H_o} - \frac{b_2^2 b_4^2}{2H_o} - Am \qquad (2)$$

$$- \frac{B^2+C^2}{4H_o}\left[\,I(I+1) - m^2\,\right] \mp \frac{BC}{H_o}\,m.$$

$$\cdots \quad \frac{1}{9}\frac{(b_2^1)^2}{H_o} + \frac{1}{10}\frac{(b_4^2)^2}{H_o} + \frac{2b_2^2 b_4^2}{H_o}$$

$$Am - \frac{B^2+C^2}{4H_o}\left[\,I(I+1) - m^2\,\right]. \qquad (3)$$

... the ... positions for the EPR lines along the x and y ... obtained, using the transformation of the crystal field ... hyperfine parameters A, B, C as worked out by ... in Table 6.

TABLE 6 Relation Between The Parameters Of The Spin Hamiltonian For Different Orientations Of The Magnetic Field H.

H || Z	H || X	H || Y
b_2^o	$-\frac{1}{2}(b_2^o - b_2^2)$	$-\frac{1}{2}(b_2^o + b_2^2)$
b_2^2	$\frac{1}{2}(3b_2^o + b_2^2)$	$\frac{1}{2}(3b_2^o - b_2^2)$
b_4^o	$\frac{1}{8}(3b_4^o - b_4^2 + b_4^4)$	$\frac{1}{8}(3b_4^o + b_4^2 + b_4^4)$
b_4^2	$-\frac{1}{2}(5b_4^o - b_4^2 - b_4^4)$	$-\frac{1}{2}(5b_4^o + b_4^2 - b_4^4)$
b_4^4	$\frac{1}{8}(35b_4^o + 7b_4^2 + b_4^4)$	$\frac{1}{8}(35b_4^o - 7b_4^o + b_4^4)$
A	B	C
B	A	A
C	C	B

The value of A is obtained by taking the average of all the hyperfine line spacings along the z-axis (25 of them). The second order terms will cancel out. Parameters B and C are obtained in a similar manner for the y and x axes.

CHAPTER IV

EQUIPMENT

The spectrometers used were of commercial design and were manufactured by Hilger and Watts Ltd., of England. The combined spectrometer system consisted of two microwave sources: one at X-band (9.4 GHz), and the other at Q-band (35 GHz), along with a common magnet, magnet power supply, detection and display systems. The microwave cavities employed were not of commercial design or manufacture. They were designed specifically for studying crystals with anisotropic properties and for this purpose they are preferable to the cavities supplied with the spectrometer. The overall system sensitivity was 10^{12} spins as the minimum required for detection and display.

A. Q-band Spectrometer

The q-band spectrometer was operated at room temperature only. It has two balanced microwave bridges, one used for signal detection and the other for frequency stabilization. The microwave source is frequency stabilized against the resonant frequency of the cavity. A block diagram of the system is shown in Figure 5. The klystron tube has a mechanical tuning range of 34.1 GHz to 35.7 GHz, (8.4 to 8.8mm free space wavelength), and electronic tuning range of 60 MHz may be accomplished by changing the reflector voltage slightly. The minimum power output for the klystron was 50 mW, with an average operation point of 60 mW.

The external magnetic field was produced by an electromagnet with a rotating base. Fields of 14 kgauss were readily obtained. Almost

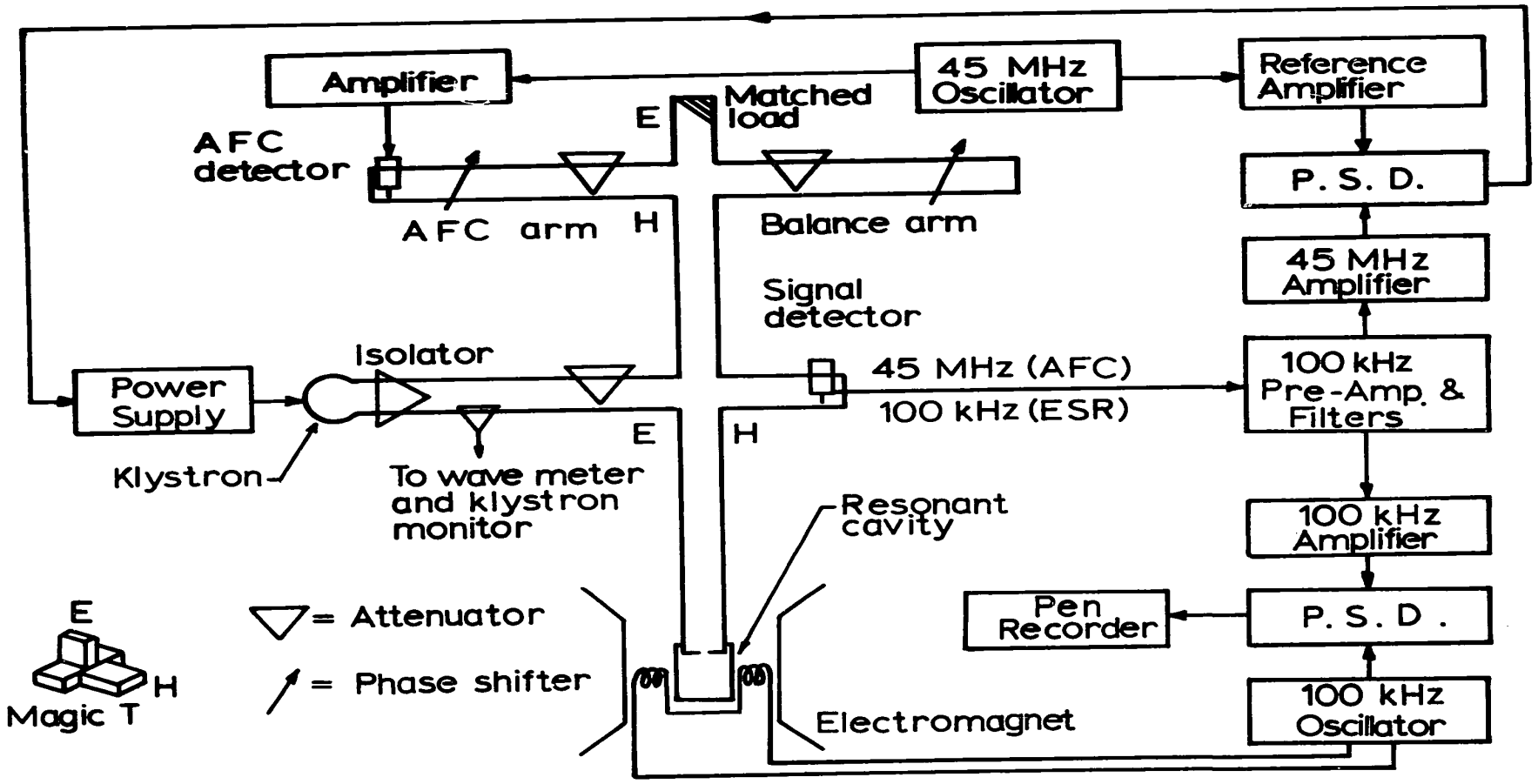

Fig. 5. Block diagram of q-band spectrometer used for ESR experiments at room temperature.

linear sweeps were available in the range. Field stability was achieved by current regulation and for steady state modes the resolution was about 200 mgauss at q-band.

The essential principles of operation are as follows. Electromagnetic energy is fed from a klystron to the first microwave bridge (magic T) where it is split equally between the side arms of the magic T. One arm feeds energy to a matched resonant cavity containing the sample, the other carries the energy to another magic T junction which reflects back a reference wave adjustable in amplitude and phase, balanced so that zero power or the low power needed to bias the crystal detector is detected in the fourth arm of the magic T junction.

In order to detect the signal it is common to modulate the external magnetic field with a small a.c. component. In this case a 100 kHz oscillator coupled to a small coil in the microwave cavity was used. Amplitude of the a.c. field was about 1 gauss.

Whenever the external magnetic field satisfied the resonance condition ($h\nu = g \beta H$) the complex susceptibility of the sample is altered, and the reflection coefficient of the cavity alters, so unbalancing the magic T bridge. The out-of-balance signal passes through a 100 kHz preamplifier, (and filters separating the ESR and AFC signals) and narrow band 100 kHz amplifier to a phase-sensitive detector. The phase sensitive detector receives its reference signal from the 100 kHz oscillator adjustable in phase relative to the modulation. The phase sensitive detector produces a derivative of the absorption signal which is shown on a strip chart recorder. The time constant of the output circuit of the phase-sensitive detector is adjustable to suit the various sweep speeds of the external magnetic field.

The second magic T enables independent setting of the bridge to

give the correct condition for the frequency stabilization of the klystron. This function, commonly referred to as AFC, (automatic frequency control) is accomplished to 1 part in 10^6. The reflected reference wave is modulated at 45 MHz in the AFC arm by the 45 MHz oscillator. Whenever the klystron frequency is different from resonant frequency of the sample cavity microwave power proportional to this difference and modulated at 45 MHz is incident on the signal detector crystal. This is transmitted after filtering, through the 45 MHz amplifier to a phase sensitive detector. The output of the phase sensitive detector is a correction voltage applied to the klystron power supply which continually tunes the klystron frequency.

B. X-Band Spectrometer

The X-band spectrometer could be operated at liquid helium, liquid air, or room temperature. Signal detection and display are achieved in the same manner as at q-band. Frequency stabilization however, is accomplished by using a transmission cavity as a reference. That is, the klystron is tuned to produce microwave power at the resonant frequency of this cavity. A block diagram of the AFC loop is shown in Figure 6. The correction voltage is proportional to the frequency difference between the reference transmission cavity and the klystron. And the sign of the correction voltage is determined by the positive or negative unbalance of the differential amplifier.

C. Q-Band Cavity

This cavity was designed and constructed specifically for the investigation of anisotropic spectra at 35 GHz. It is cylindrical in shape and operates in the TE_{011} mode. The system is shown in Figure 7.

The dimensions for a cylindrical cavity operating in the TEmnp mode are determined from the formula:

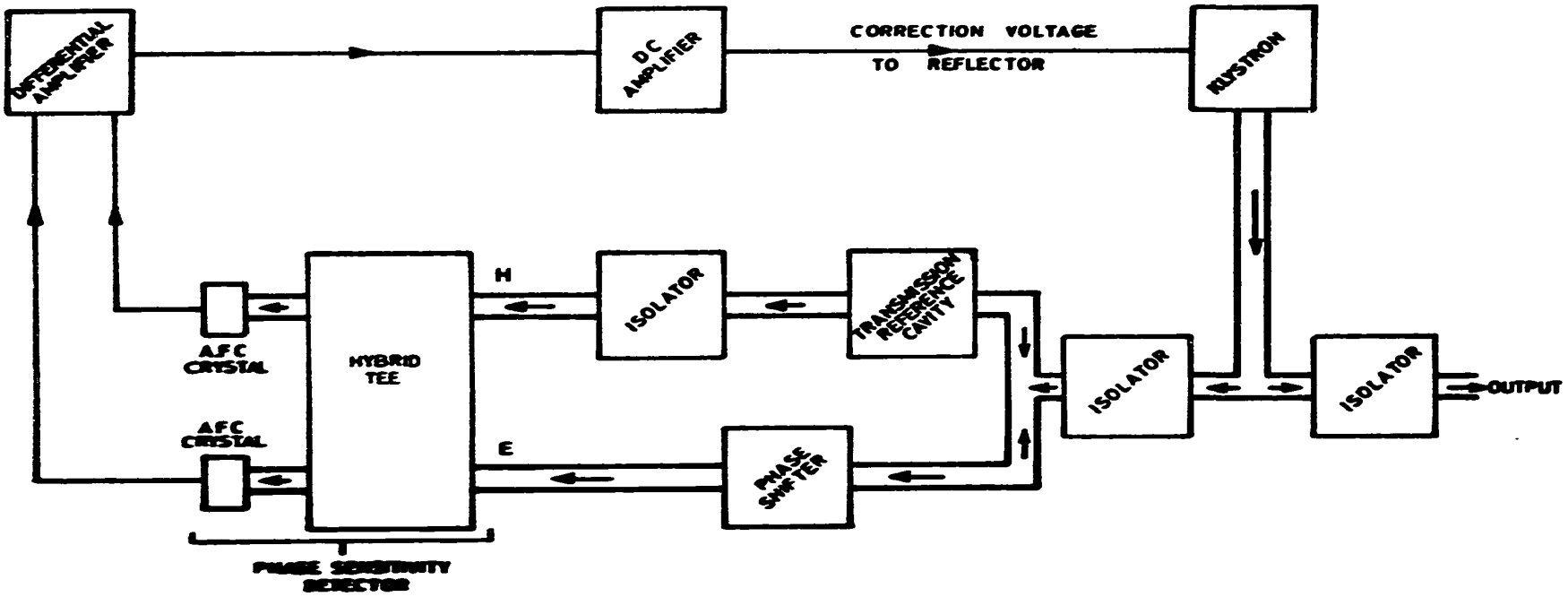

Fig. 6. Automatic frequency control loop in the x-band spectrometer.

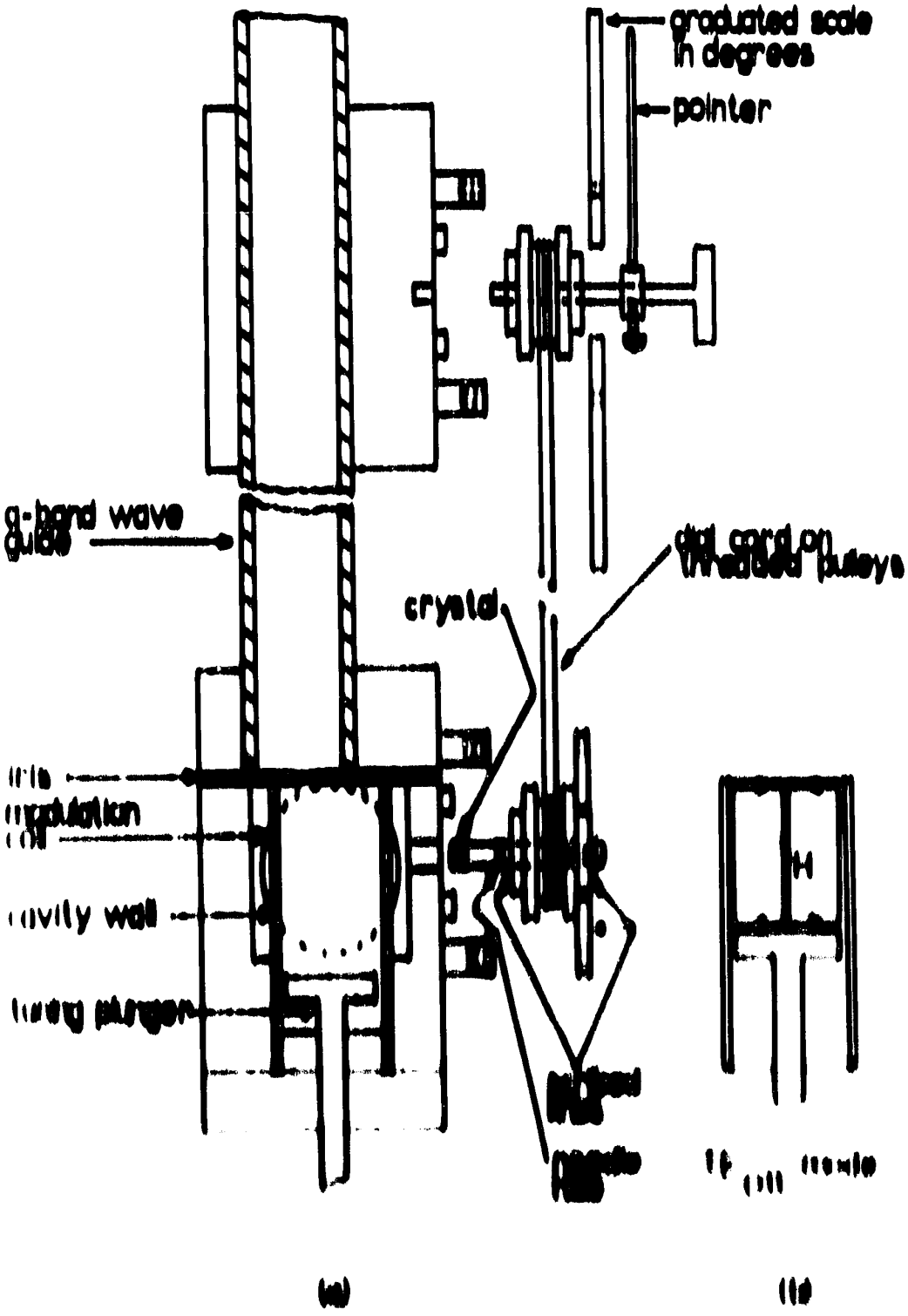
graduated scale in degrees
pointer
g-band wave guide
crystal
iris
cavity wall
(a)
(b)

$$k_0 = \frac{2\pi}{\lambda_0} = \left[\frac{(k_{ca})^2_{mn}}{a^2} + \left(\frac{l\pi}{2h} \right)^2 \right]^{1/2}$$

where, λ_0 is the free space wavelength,

a is the radius of the cavity,

$2h$ is the height of the cavity,

$(k_{ca})_{mn}$ is the nth root of equation $\frac{d}{dr} Jm\,(k_{cr})_{r=a} = 0$

and Jm is a Bessel function of order m.

The subscript m, n, and p give number of one half wavelengths in the ϕ, r, and z directions respectively, where ϕ, r, and z are the coordinates of a point in the cylindrical frame of reference. For the H_{111} mode, $(k_{ca})_{011} = 3.83/$, and with this substitution the above equation can be simplified to,

$$k_0 = \left[\left(\frac{3.83}{a} \right)^2 + \left(\frac{\pi}{2h} \right)^2 \right]^{1/2}$$

It can be shown[11] that for [illegible]

the tuning plunger and the conductive lining as shown in Figure 7.

The cavity is coupled to the waveguide through an iris .005 inches thick. The optimum aperture diameter for the iris is dependent on the sample shape to some extent and is best determined by trying apertures of different diameters. A diameter almost equal to the small dimension of the waveguide was found satisfactory for most samples investigated.

The external magnetic field is modulated by two Helmholtz coils, one of which is shown in the figure. The modulation frequency is 100 kHz and to ensure modulation of the sample the conductive layer of the cavity must be thin. The cavity wall is made of perspex one thirty-second of an inch thick. The inner wall is lined with aluminum foil of [illegible] thickness. This is quite sufficient for propagation of microwave energy at 10 kHz since the skin depth at that frequency is about [illegible] for most conductors. The penetration of the 100 kHz field [illegible] and large signals were obtained for samples [illegible] mounted

[illegible] on a perspex pin which is fastened to the [illegible] the cavity is axially coupled to a vertical [illegible] rotated the sample in a vertical plane [illegible] the external magnetic field is [illegible] rotating the magnet an angle ϕ on its [illegible] cavity system to align the magnetic [illegible]

[illegible] unambiguously, a system of [illegible] in the perspex pin pur- [illegible] two slots in the pin could [illegible] the pulley adjacent to

the cavity. After tightening the screw which holds the pin in the pulley, the entire assembly could be turned so as to line up the scribed lines, one on the pulley and the other on the retaining plate.

This method allows the removal of the sample and pin from the cavity for X-ray work or other analysis. The needle hole and the pin axis with respect to magnet position define the angles θ and ϕ. As long as the sample is not removed from the pin, placement in any previous orientation in the cavity is possible.

As stated in Chapter II, (B), the X-ray analysis was carried out by fastening the pin with attached sample to a Philips goniometer with two degrees of freedom, rotation in vertical plane, angle θ, and rotation in horizontal plane, angle ϕ. Thus it was possible to correlate the crystallographic axes of the crystal, as found by X-ray analysis, with the magnetic axes of the Mn^{+2} complexes, as found by ESR measurements.

D. X-Band Cavity

This cavity was rectangular and operated in the TE_{012} mode. A diagram of this system is shown in Figure 8. The sample was again mounted so that it could be rotated in a vertical plane (agnle θ). In this case, the rotation is accomplished by worm and worm gear arrangement as shown. The 100 kHz magnetic field modulation loop is provided by a single turn of copper wire placed at the center of the cavity. The end of the loop is bent aside in order to clear the crystal hole on the side of the cavity.

E. Magnetic Field Measurement

Nuclear magnetic resonance of hydrogen protons in water was used to measure the magnetic field at which ESR transitions occured. For this purpose water doped with a small amount of copper sulphate was

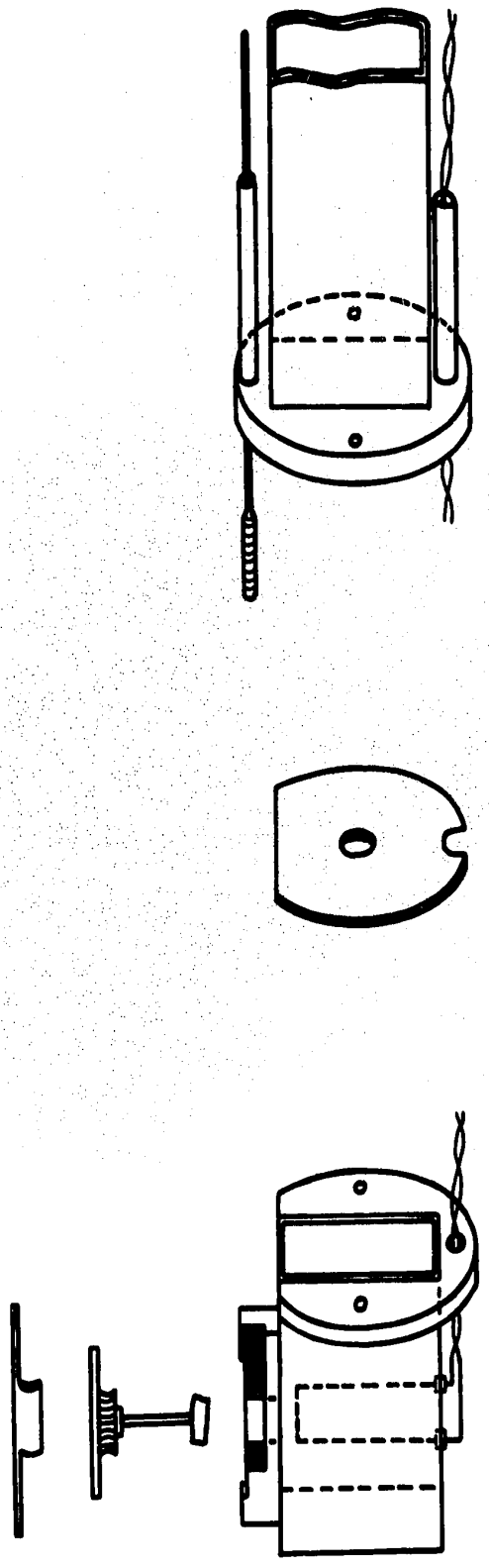

Fig. 8. X-band rectangular cavity system with horizontal crystal mount. Rotation of specimen is by worm and gear.

used. The nuclear absorption signal was observed on an oscilloscope, with the signal fed to the vertical imput and a 60 Hz signal with a phase shifter applied to the horizontal imput. The magnetic field was also modulated at 60 Hz. For a given magnetic field, the frequency applied to the coil containing the sulphate solution was varied until an absorption line appeared on the oscilloscope. The frequency at resonance was measured with a Hewlett Packard No. 52533 frequency counter. The magnetic field was calculated from the formula.

$$H\ (\text{kgauss}) = \frac{\nu\ (\text{MHz})}{4.25759}$$

where, ν is the proton resonance frequency, and 4.25759 is the frequency in MHz for proton resonance at 1000 gauss.

F. Microwave Frequency Measurement

The microwave frequency for any ESR spectrum could be obtained by introducing a trace of DPPH* on the crystal. The ESR transition due to DPPH was easily discernable by its intensity and narrow line width from Mn^{+2} spectra. First the magnetic field at DPPH resonance is measured as described previously. The microwave frequency in the cavity is calculated from

$$h\nu = g\beta H$$

where, h is Plank's constant (6.62517×10^{-27} erg-sec),

g is 2.0036 for DPPH,

β is the Bohr magneton (0.92731×10^{-21} erg/gauss),

H is the resonant magnetic field for DPPH in gauss,

ν is the desired frequency in Hz.

* DPPH stands for diphenyl picryl hydrazyl.

CHAPTER V

EXPERIMENTAL PROCEDURE AND RESULTS

The ESR spectra of Mn^{+2} in monticellite were analyzed at both x- and q-band microwave frequencies, but most of the final measurements were made at q-band. Many samples of monticellite were investigated and all gave similar spectra. Investigations at liquid helium temperatures ($4.2^{o}K$) were also attempted, at x-band frequencies, but the ESR lines were poorly resolved and so no conclusive work could be done at low temperatures.

A. Determination Of The Magnetic Axes At X-Band

The magnetic axes of the Mn^{+2} magnetic complexes were first determined at x-band frequencies using the rectangular cavity system shown in Figure 8. The magnet angle ϕ and the crystal angle θ were varied in steps of about 5^{o}. A recording of the spectra was obtained each time on the strip-chart recorder. It soon became evident that there were four complexes of Mn^{+2} with each complex consisting of five groups of six hyperfine lines for a total of thirty lines each, as is characteristic of divalent manganese. There were also numerous forbidden transitions of Mn^{+2}, which presumably obeyed the selection rules $\Delta M_S = \pm 1$, $\Delta m_I = \pm 1$.

The magnetic axes of a given complex are obtained when the five groups of six hyperfine lines show extrema in their separation. This occurs when the external magnetic field points along the three perpendicular axes of the crystal field tensor. The Z axis is defined as

the direction of greatest separation of the hyperfine groups for a given complex. The Y axis is 90° away from the Z axis and the groups of lines have a smaller separation in this direction. The X axis is mutually orthogonal to the Y and Z axes and the groups show an even smaller separation in this direction. In fact, the hyperfine lines overlapped to such an extent in the X direction that it was not possible to make any quantitative measurements along this direction. The spectra were studied in detail along the Z and Y directions.

The four complexes discovered were observed to have not four but two sets of magnetic axes. That is the four complexes went through their extrema in pairs. The two sets of magnetic axes were designated with subscripts 1 and 2, and their directions are plotted on a stereographic projection net in Figure 9. Shown also in the same figure are the directions of the crystallographic axes as determined by X-ray analysis. The angular relationships between the crystallographic and magnetic axes can be expressed in terms of rotation matrices as follows:

$$\begin{bmatrix} x_1 \\ y_1 \\ z_1 \end{bmatrix} = \begin{bmatrix} \cdot & \cdot & \cdot \\ \cos 41 & \cdot & \cdot \\ \sin 41 & \cdot & \cdot \end{bmatrix} \begin{bmatrix} \cdot \\ \cdot \\ \cdot \end{bmatrix}$$

$$\begin{bmatrix} x_2 \\ y_2 \\ z_2 \end{bmatrix} = \begin{bmatrix} \cdot & \cdot & \cdot \\ \cdot & \cdot & \cdot \\ \cdot & \cdot & \cdot \end{bmatrix} \begin{bmatrix} \cdot \\ \cdot \\ \cdot \end{bmatrix}$$

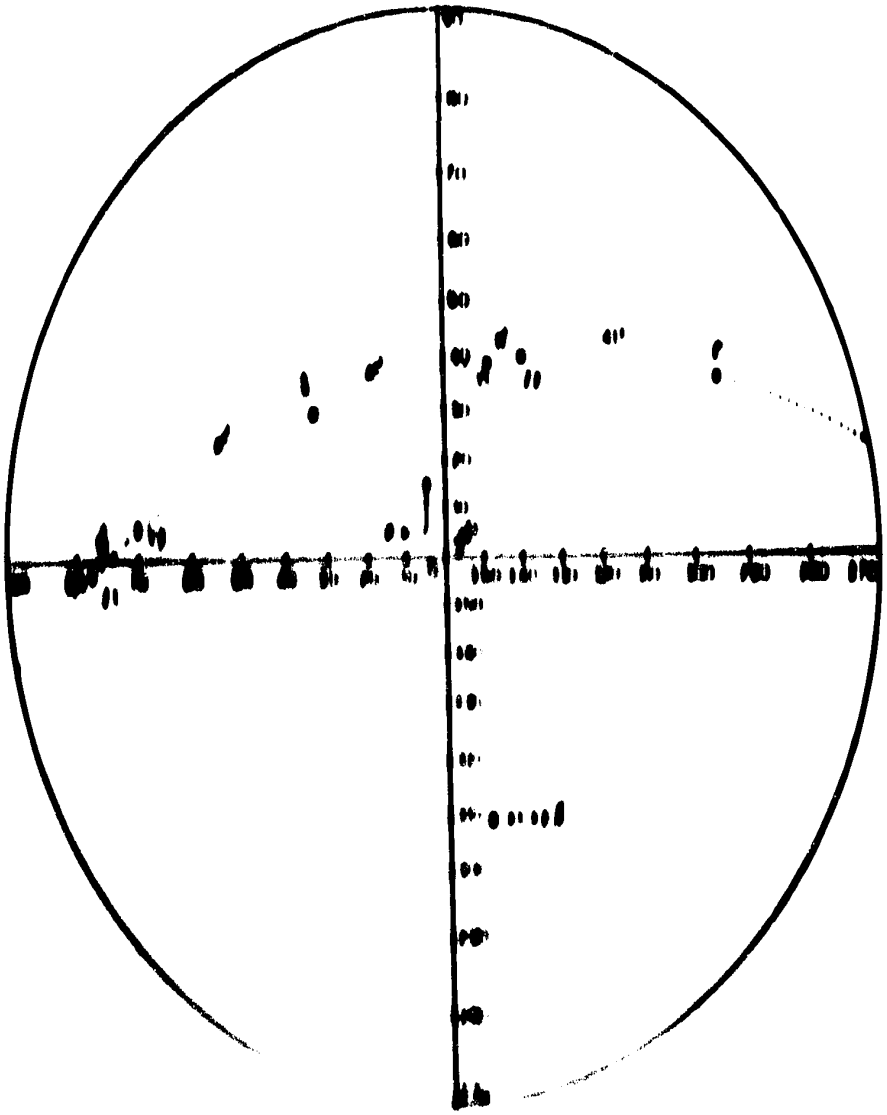

where, $\vec{i}$, $\vec{j}$, $\vec{k}$ are unit vectors along $\vec{a}$, $\vec{b}$, and $\vec{c}$ respectively and $\vec{x}_1$, $\vec{y}_1$, $\vec{z}_1$, $\vec{x}_2$, $\vec{y}_2$, $\vec{z}_2$ are unit vectors along X_1, Y_1, Z_1, X_2, Y_2, and Z_2 respectively.

Magnetic field positions along the Z_1 and Z_2 directions, for the hyperfine lines $m = \pm 5/2$ were measured and the results are shown in Table 7.

TABLE 7 Magnetic Field Values For Z_1 And Z_2 At X-Band

Position	Z_1 (gauss)	Z_2 (gauss)	Difference (gauss)
H_1	1119.9 ± .1	1114.7 ± .1	1.2
H_2	1566.8	1569.0 "	1.8
H_3	2087.3 "	2089.0 "	2.3
H_4	2929.0 "	2928.7 "	1.1
H_5	3093.3	3090.7 "	2.6
[illegible]	3401.2	3402.6	1.4
H_6	3924.5	3929.9 "	5.6
H_7	4109.0	4104.5	.5
H_8	4610.0	4608.2 "	1.6
H_9	9460.6	9499.7	8.9
H_{10}	9879.9	9844.2	35.0

It is seen that magnetic field values for equivalent transitions were within a few gauss of each other in almost all cases. The spectra obtained for Z_1 and Z_2 were identical in appearance, they are inclined at 41° to the c axis. The Z_1 spectrum is shown in figure 10

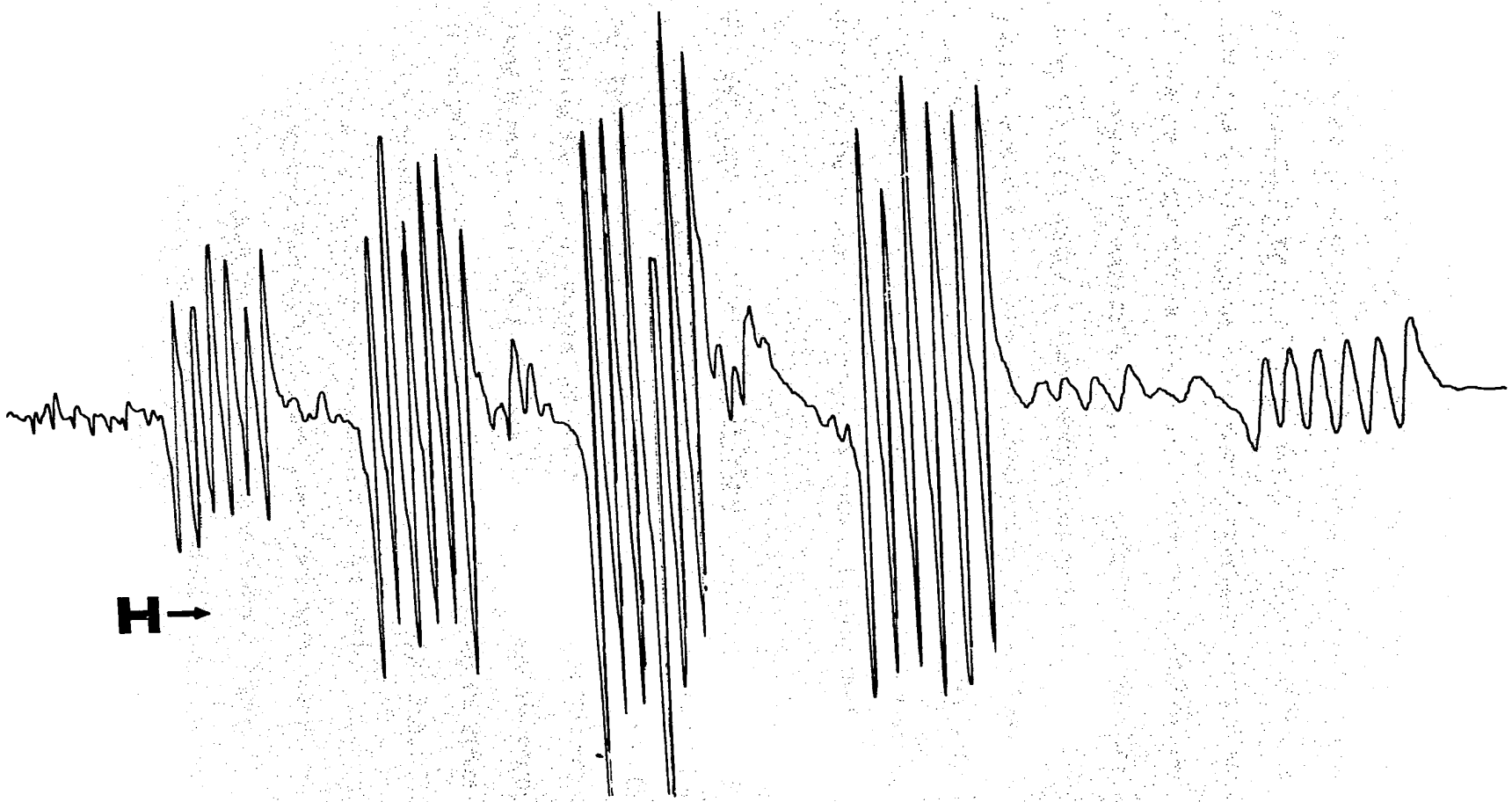

Fig. 10. The spectrum of Mn^{+2} in monticellite at x-band with the magnetic field along a Z axis.

Identical spectra were also observed for the Y_1 and Y_2 directions. These are seen to be in the plane defined by the directions Z_1 and Z_2, which is also the crystallographic (010) plane. The Y_1 and Y_2 axes are 8^o away from the Z_2 and Z_1 axes respectively. As these directions are quite close to the Z axes one would expect to observe 60 lines alltold; 30 lines due to the Y of one complex and 30 lines due to the Z of the other complex. It turned out however, that in addition, numerous forbidden lines were observed. Consequently it was quite difficult to identify some of the hyperfine lines unambiguously along the Y axes. Hence it was decided to study the spectra at Q-band frequencies in the hope that the forbidden lines would diminish in intensity and thus facilitate the resolution of the spectra, especially along the Y axes.

B. Determination Of Magnetic Axes At Q-Band

The specimen was attached to a perspex pin, this time with the pin axis parallel to the crystal $\vec{b}$ axis. This orientation was confirmed by measuring the crystal parameter parallel to the pin axis and this was found to correspond to the b unit cell dimension. At Q-band the cylindrical cavity shown in Figure 7 was used. With this set-up the direction of the external magnetic field was varied in the (010) crystal plane simply by turning the threaded pulleys on the cavity.

The magnetic axes Z_1, Y_1, Z_2, and Y_2 were once again located. Typical spectra along the Z and Y directions are shown in Figure 11 and 12 respectively. The same angular relationships between the spectra and the crystallographic axes were found to hold as at X-band. As hoped many forbidden lines previously observed either were not observable or decreased in intensity considerably so that it was possible to resolve the spectra along the Y directions. Magnetic field values for the

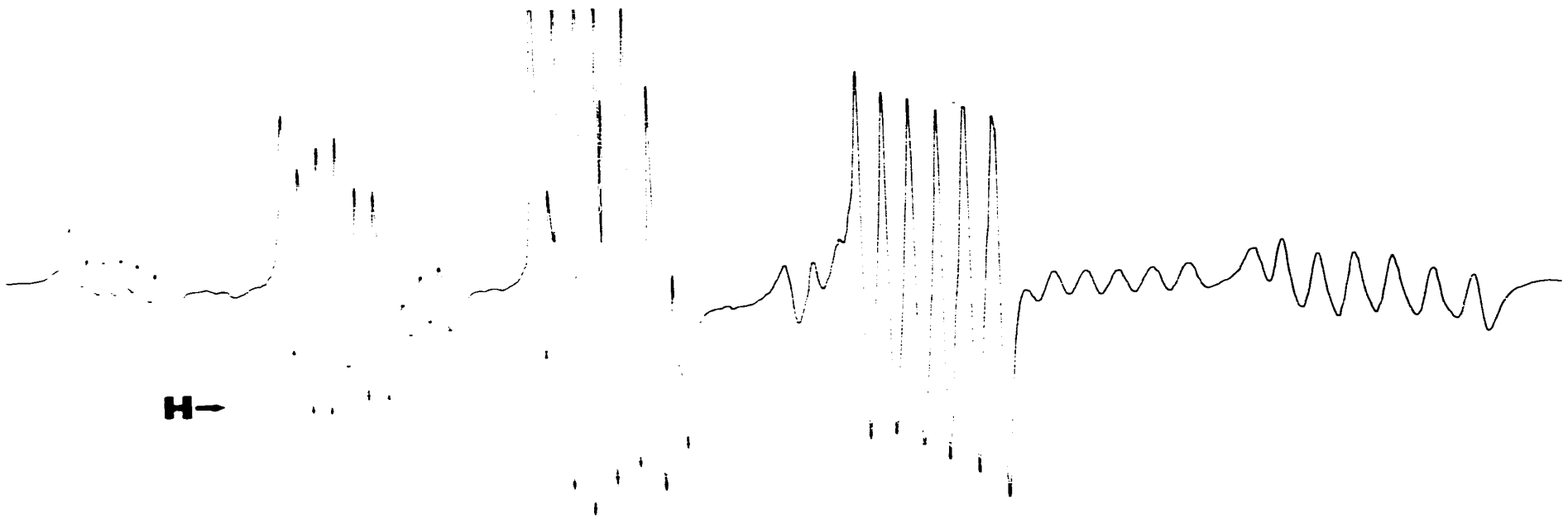

Fig. [illegible] The spectrum of Mn^{+2} in monticellite at q-band with the magnetic field along a Z axis.

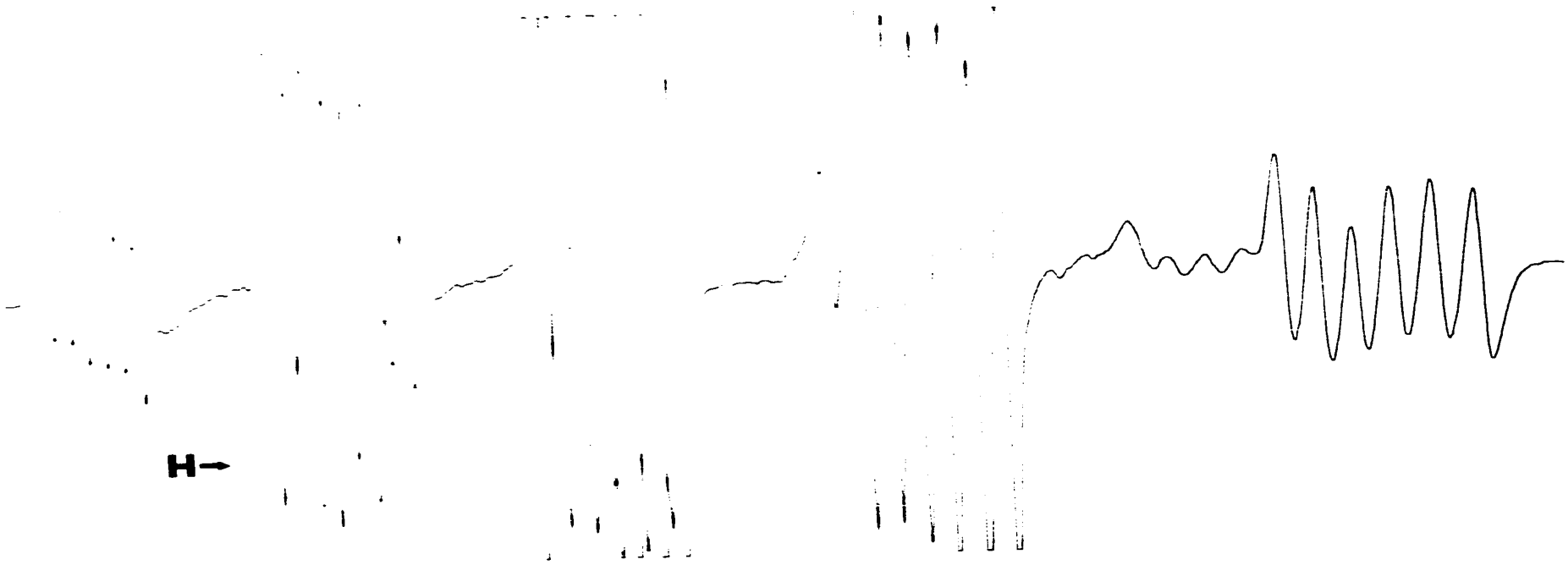

Fig. 12. The spectrum of Mn^{+2} in monticellite at q-band with the magnetic field along a Y axis.

m = ± 5/2 lines for the spectra in Figures 11 and 12 were measured and the results are shown in Table 8.

TABLE 8 Magnetic Field Values For m_I = ± 5/2 Transitions Along The Z And Y Axes At Q-Band

Position	Z Axis (gauss)	Y Axis (gauss)
H_1	9590.5 ±.1	10122.9 ± 1
H_2	10007.1 ± 1	10516.2 "
H_3	10656.7 "	10812.0 "
H_4	11078.3 "	11224.6 "
H_5	11815.1 "	11765.3 "
DPPH	11988.5 "	11991.1 "
H_6	12250.0 "	12185.1 "
H_7	12882.1 "	12758.3 "
H_8	13305.1 "	13214.6 "
H_9	14057.1 "	13671.7 "
H_{10}	*	14148.5 "

* not attainable with available magnet power supply.

C. Calculation Of Spin Hamiltonian Parameters

The parameters b_n^m, A, and B were found from equations 1, 2, and 3 using the magnetic field positions for the hyperfine lines given in Table 8. The results are shown in Table 9.

TABLE 9 The Spin Hamiltonian Parameters For Mn^{+2} In Monticellite

Parameter	Value
g_z	1.9901 ±.0010
g_y	1.9905 ±.0010
A	85.5 ± 2
B	85.5 ± 2
b_2^0	-558.5 ± 1
b_2^2	-351.7 ± 1
b_4^0	-0.500 ±.001
b_4^2	-56.0 ±.1
b_4^4	-40.3 ±.1
H_{oz}	12033.6 ± 1
H_{oy}	12069.8 ± 1

The values of b_n^m, A, B, H_{oz}, and H_{oy} are in gauss.

Using the values of the constants in the above table, the matrix of the spin Hamiltonian was diagonalized for incremental values of magnetic field. The field was varied in steps of 100 gauss from zero field to 15000 gauss. The calculations were done on an IBM 360 computer utilizing a library diagonalization subroutine. Values thus obtained were used to plot the energy level diagram which is shown in Figure 13.

D. Angular Variation Of The ESR Spectra In The (010) And (001) Planes

Partial angular variation of the m = 5/2 hyperfine lines was carried out in the (010) plane first. The results are shown in Figure 14.

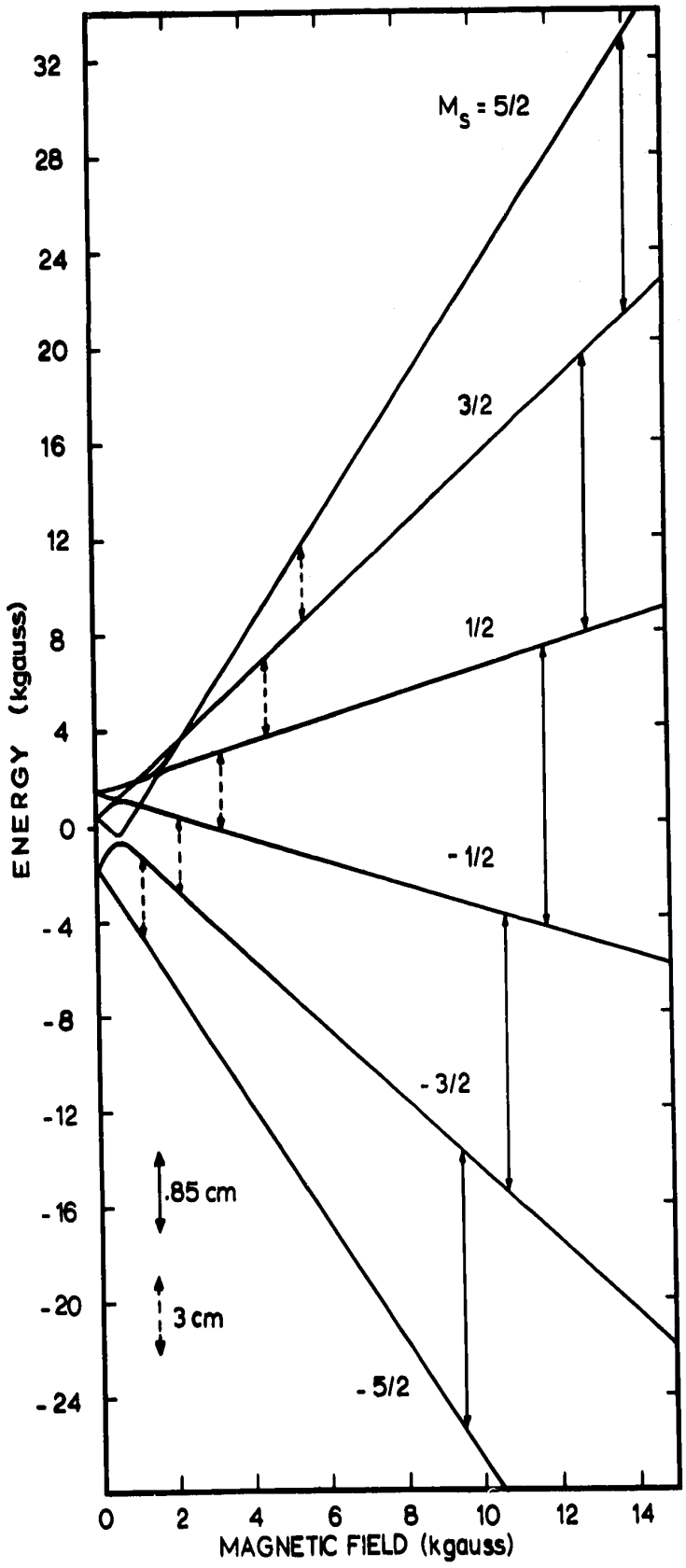

Fig. 13. Energy level diagram of Mn^{+2} in monticellite with the magnetic field along a Z axis. The vertical transitions show the centers of gravity of the hyperfine lines at x and q-band frequencies as indicated.

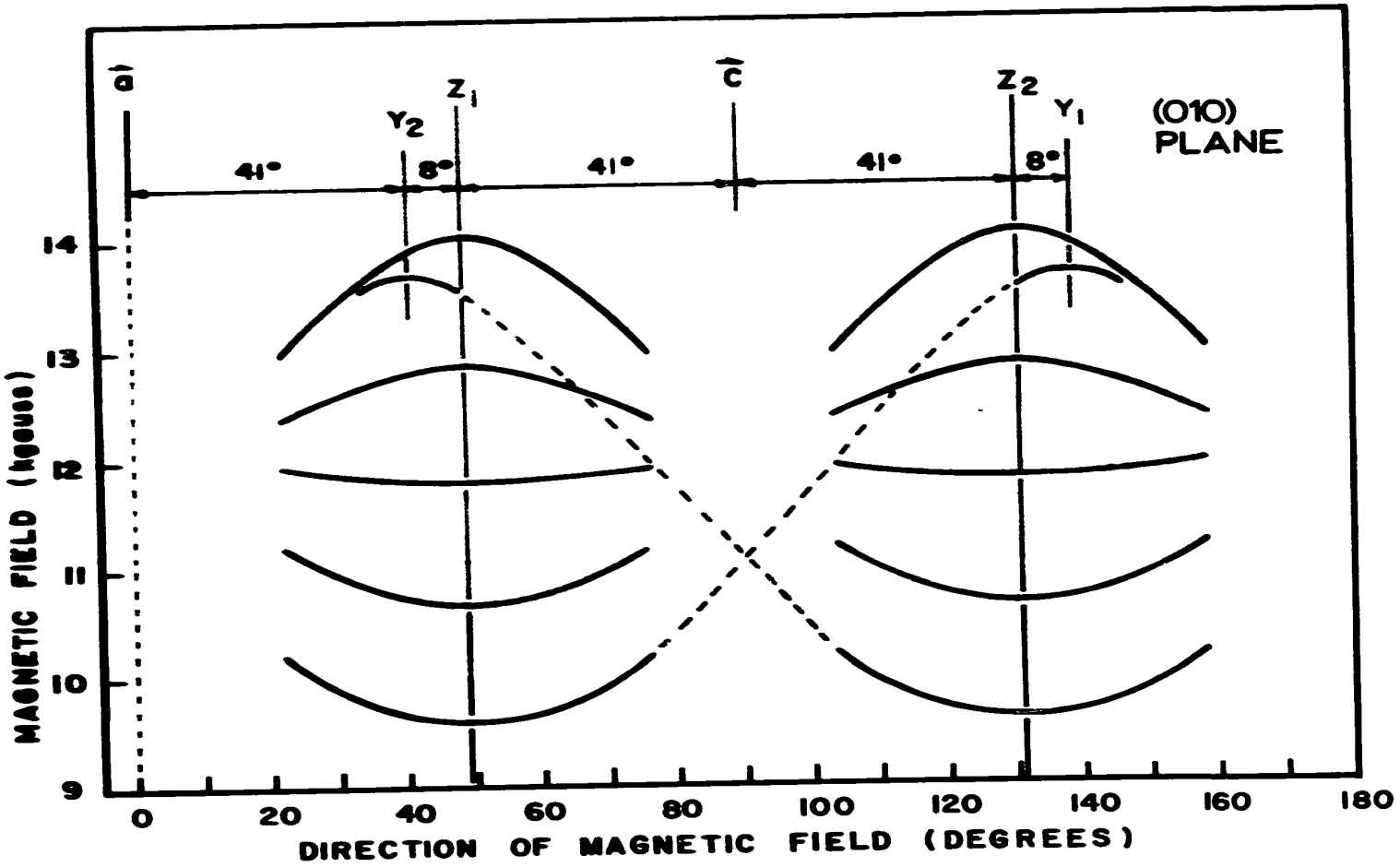

Fig. 14. Partial angular variation of Mn^{+2} complexes in (010) for $m_I = 5/2$.

It can be seenthere that the two Mn^{+2} complex pairs behave identically in this plane. This follows from the equal magnetic field values and the identical angular variation of the m = 5/2 lines of the complexes. Also shown in the figure is partial angular variation of the m = 5/2 line for the top group about the Y axes.

When the magnetic field was 3^{o} or more off the (010) plane, it was observed that each group of hyperfine lines, consisting of six lines, split into two groups, consisting of twelve lines. This effect is shown in Figure 15 for one group of hyperfine lines. This means that there are actually four complexes of Mn^{+2} closely related in pairs. And, as seen in the (010) plane, they degenerate into two complexes.

The same specimen as used above was also oriented with the perspex pin along the crystallographic $\vec{c}$ axis so that turning of the pulleys would vary the direction of the magnetic field in the (001) plane. The spectra observed in this plane were poorly resolved, and the maximum separation of the group of hyperfine lines was considerably less than any exrema in the (010) plane.

E. Accuracy In Results

The uncertainty in all angular measurements is believed to be no more than two degrees. This figure is chosen as the upper limit since all angular relationships have been redetermined a number of times and in all cases repeatability was within 2^{o}. In particular the angular separation between Z_1 and Z_2 in the (010) plane, (= 82^{o}), is believed to be within this limit.

The uncertainty in magnetic field measurements is estimated to be ± .1 gauss. This value is obtained as follows. The magnetic field in gauss is calculated from $\nu \times 10^{3} / 4.25759$. Where ν is the frequency

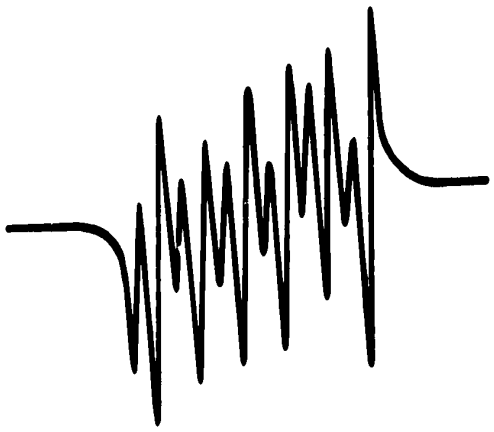

Fig. 15. Splitting of a group of hyperfine lines of Mn^{+2} from six to twelve for the magnetic field about 3^{o} off the (010) plane.

In MHz for proton resonance at a given field. The uncertainty in H is therefore determined by the instability in proton resonator frequency. This was about 100 Hz for frequencies of 10 MHz, (1 part in 10^5). On the basis of this the uncertainty in H is one part in the fifth significant figure or ± .1 gauss for values in Tables 7 and 8. The stability of the field itself was in the milligauss range and consequently is well within this limit.

Although the field values were measured within a tenth of a gauss this does not mean that the values given in Tables 7 and 8 are to be associated with the ESR transitions indicated there to the same accuracy. The line widths involved were too large for this. The uncertainty in the line positions is estimated to be several gauss, or several parts in the fourth significant figure in Tables 7 and 8. This implies in turn, at most, an uncertainty in the spin Hamiltonian parameters of one part in the third significant figure.

CHAPTER VI

DISCUSSION AND CONCLUSIONS

A. Correlation Of ESR Results With Crystal Structure Of Monticellite

The ESR signals in monticellite are due to divalent manganese. This is evident from the spectra observed and the fact that the ground state term for Mn^{+2} is $^6S_{5/2}$.

It is possible to correlate the observed spectra with cation sites in monticellite. The two complexes, which in reality are four complexes in pairs, exhibit identical behaviour in the (010) plane. This means that both complexes must be produced by crystallographically equivalent neighbourhoods. Examination of the cation sites projected on the (010) plane in Figure 3 shows two sets of four equivalent neighbourhoods. One set is the magnesium sites α, $\bar{\alpha}$, β, and $\bar{\beta}$. The other set is the calcium sites γ, $\bar{\gamma}$, δ, and $\bar{\delta}$. On the basis of the above, it is clear that manganese spectra could originate from one set of sites or the other but not from both since they are not crystallographically equivalent. With the aid of symmetry considerations however, it is possible to further exclude one of these as follows. The orthorhombic spectra are found to have one set of magnetic axes (the X_1 and X_2 axes) along the [010] direction. Thus the other two axes are in the (010) plane. Now since the spectra are orthorhombic, they must be due to paramagnetic impurities in sites which have two-fold rotation symmetry in that plane. Again, examination of Figure 3 shows that only sites α, $\bar{\alpha}$, β, and $\bar{\beta}$ have this property. Thus the conclusion can be

drawn that manganese in monticellite substitutes for magnesium and does not do so for calcium. The latter conclusion is subject to the following qualification. If calcium sites are substitutionally occupied by manganese their number is less than 10^{12} for the specimens investigated. This limit is determined by the sensitivity of the spectrometers. There are no reasons, however, to believe that this is the case.

It is to be noted that the Z axes are inclined to the $\vec{c}$ axis at 41° in the (010) plane, and that these directions are along the oxygen bond projections in that plane. This fact confirms that manganese enters monticellite substitutionally and not interstitially. The correlation of ESR spectra with the crystal structure is completed by attributing one paired complex to the sites α, $\bar{\alpha}$, and the other paired complex to the sites β and $\bar{\beta}$. This association is indicated by the fact that sites $\bar{\alpha}$ and $\bar{\beta}$ are obtained by reflection of the α and β sites respectively in the (010) plane. Thus for magnetic fields in (010) α and β are equivalent to $\bar{\alpha}$ and $\bar{\beta}$ respectively. It follows, therefore, that one paired complex is due to α and $\bar{\alpha}$ and the other paired complex is due to β and $\bar{\beta}$ sites.

The magnetic Z axes, as shown in Figure 3(a), are coincident with oxygen bond directions. It will be recalled that this is for the structure of monticellite (based on the forsterite structure) according to Bragg and Claringbull. The angles shown there would both be about 36° for oxygen coordinates in the original structure determination by Brown and West. If the latter structure is assumed correct, there is approximately a 5° difference between oxygen bond projections and magnetic Z axes in the (010) plane. This in itself is a possible result as long as the ESR spectrum has two-fold rotation symmetry in that plane. Frequently, however, magnetic axes,

especially the Z axes, point through nearest ligands or along ligand bond projections. It seems most probable, therefore, that a redetermination of the structure of monticellite is in order if precise location of atoms in the unit cell is required. Recently, many structure determinations have been redone and differences with the original work have been found. Two minerals, which are isomorphous with monticellite and whose structures have recently been redetermined are, forsterite[8] and chrysoberyl[18].

B. Comparison Of This Work With Few Other ESR Studies Of Natural Minerals

It is of interest to compare relative magnitude of spin Hamiltonian parameters for a given impurity in different magnetic complexes but of same overal symmetry. This is done in Table 10 for a few minerals recently studied.

TABLE 10 Spin Hamiltonian Parameters Of Mn^{+2} In Orthorhombic Complexes Of Some Minerals

Mineral		Cubic Term	Axial Terms		Orthorhombic Terms	
		b_4^4	b_2^o	b_4^o	b_2^2	b_4^2
Tremolite[19]	pink	-34.6	-448.3	-0.96	-234.7	33.0
Monoclinic	white	18.2	-442.9	-0.43	-238.1	-19.0
$2(H_2Ca_2Mg_5(SiO_3)_8)$						
Diopside[6]	Mg site	15.88	452.95	0.34	-308.5	-4.74
Monoclinic	Ca site	32.42	373.84	-6.58	51.26	-2.93
$(CaMgSi_2O_6)$						
Monticellite	Mg site	-40.3	-558.2	-0.5	-351.7	-56.0
Orthorhombic	Ca site	*				
$(CaMgSiO_4)$						

* No ESR spectrum detected. In tremolite it is not known whether Ca or Mg sites are responsible for ESR signals.

Examination of the table shows, for example, that the Ca sites in diopside are more symmetric than the Mg sites in the same mineral since the former has a larger cubic term and smaller axial and orthorhombic terms. Monticellite is seen to have axial and orthorhombic terms which are larger than the corresponding terms both in diopside and tremolite. It appears then, that the magnesium sites there have larger distortions from cubic symmetry than similar sites in diopside and tremolite.

It has been shown that the hyperfine constant A is related to amount of covalent bonding[20], the greater the covalent bonding the smaller the hyperfine splitting. Matumura[21] has obtained a graph which shows an almost linear relationship between the coupling constant A and the ionicity. On the basis of his graph, tremolite, monticellite, and diopside have 86, 91, 91 (Mg site) and 95 (Ca site) per cent ionicity, respectively.

It has been mentioned that chrysoberyl (Al_2BeO_3) is isostructural with monticellite and that for this reason it is of interest to compare ESR results in the two minerals. Best for this purpose would be results due to a common impurity. Unfortunately, the only reported paramagnetic ion in chrysoberyl is Fe^{+3}. The equivalent of $\overline{\alpha}$ and $\overline{\beta}$ sites in monticellite are shown for chrysoberyl in Figure 16 and Table II summarizes some results obtained for the minerals.

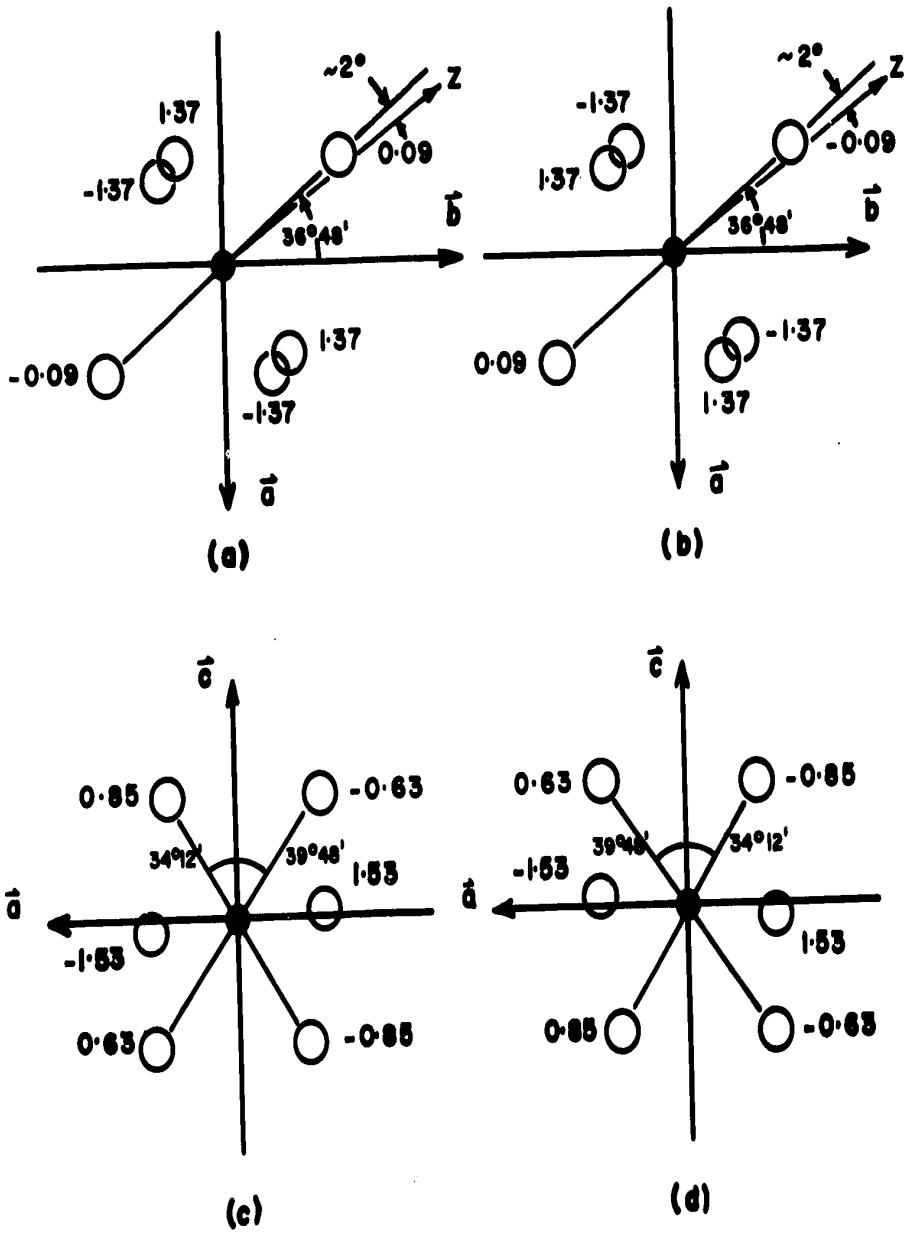

Fig. 16. $\bar{\alpha}$ and $\bar{\beta}$ sites in chrysoberyl are shown in (c) and (d) respectively, projected on (010). (a) and (b) show the sites in (c) and (d) respectively, projected on (001). The full circles are aluminum and the surrounding atoms are oxygen. The scale is 1/4" = 1A and elevations are above and below paper plane. The sites are based on the refined structure of chrysoberyl[18].

TABLE II Comparison Of Some ESR Results In Monticellite And Chrysoberyl

	Monticellite ($CaMgSiO_4$)	Chrysoberyl (Al_2BeO_3)
Impurity	Mn^{+2}	Fe^{+3}
Replaces	Mg Yes Ca No	Al_1 Yes * Al_{11} No
No. of Complexes: Expected on basis of symmetry	Four in pairs	Four in pairs
Actually observed	Two in pairs	Two in pairs
Spectrum symmetry	Orthorhombic	Orthorhombic
Two magnetic axes in	(010) plane	(001) plane

* Al_1 are inversion centers and correspond to Mg in monticellite, Al_{11} correspond to Ca sites in monticellite.

Vinokurov et al[7] have found two magnetic axes for each paired complex in (001). On the basis of the chrysoberyl structure their Z axes are along oxygen-aluminum bond projections in this plane. The angle between this projection and [010] is about 35° in the old structure and about 37° in the refined structure. So that the magnetic Z axes no longer point through the oxygen atoms. It is interesting to note that angles close to 35° (34° - 12') may also be found in the

(010) plane, and also that in this plane the sites have two-fold rotation symmetry as is shown in Figure 16 (c) and (d). This means that on the basis of symmetry alone, the orthorhombic Fe^{+3} spectrum could have two of its magnetic axes in the (001) plan , as reported, or in the (010) plane as is the case for monticellite. Vinokurov et al, unfortunately, do not state without ambiguity how their results were obtained. Nor do they mention the possibility of magnetic axes in (010) plane, a purely theoretical consideration, of which apparently they were not aware. It is not entirely out of the question, therefore, that their magnetic axes were in the (010) and not in the (001) plane. If this were the case, the analogy in Table II would be complete. It would be interesting to pursue this question further, especially in chrysoberyl containing Mn^{+2} impurity.

In conclusion, it is pointed out that as far as is known, monticellite is the only member of the olivine group of minerals which has been studied via ESR. The entire group could be studied from this point of view, since the remaining three members; forsterite, fayalite, and tephroite and their various solid solutions should all exhibit ESR signals.

LIST OF REFERENCES

1. J.H. Van Vleck and W.G. Penney, Phil. Mag. 17, 961 (1934).
2. A. Abragam and M.H.L. Pryce, Proc. Roy. Soc. A205, 135 (1951).
3. J.R. Gabriel, D.F. Johnson and M.J.D. Powell, Proc. Roy. Soc. A264, 503 (1961).
4. P.B. Ayscough, Electron Spin Resonance In Chemistry (Methuen and Co. Ltd., London) (1967).
5. W. Low, Advances In Electronics And Electron Physics 24, p.51 (1968).
6. V.M. Vinokurov, M.M. Zaripov and V.G. Stepanov, Soviet Phys. Solid State (English Transl.) 6, 870 (1964).
7. V.M. Vinokurov, M.M. Zaripov, V.G. Stepanov, Yu.E. Pol'skii, G.K. Charkin and L.Ya. Shekun, Soviet Phys. Solid State (English Transl.) 3, 1797 (1962).
8. W.L. Bragg and G.F. Claringbull, Crystal Structures Of Minerals (G. Bell and Sons, Ltd., London), p.173 (1965).
9. G.B. Brown, J. West, Zeitschr f. Krist. 66, 154 (1928).
10. H. Bethe, Ann. Physik 3, 133 (1929).
11. E. Wigner, Nachr. Akad. Wiss. Gottingen, Math.-physik Kl. II a, 546 (1932).
12. M.H.L. Pryce, Proc. Phys. Soc. A63, 25 (1950).
13. R. Orbach, Proc. Roy. Soc. A264, 458 (1961).
14. K.W.H. Stevens, Proc. Phys. Soc. A65, 209 (1952).
15. D.A. Jones, J.M. Baker and D.F.D. Pope, Proc. Phys. Soc. 74, 249 (1959).
16. W. Low, Paramagnetic Resonance In Solids (Academic Press, New York) (1960).

17. C.P. Poole Jr., Electron Spin Resonance, p. 268, 271, 273, 274. (Interscience Publishers) (1967).

18. E.F. Farrell, J.H. Fang, R.E. Newnham, The American Minerologist, 48, 804 (1963).

19. A. Manoogian, Can. J. Phys., 46, 129 (1968).

20. J.S. Van Wieringen, Disc. Farad. Soc., 19, 118 (1955).

21. O. Matumura, J. Phys. Soc. Japan, 14, 108 (1959).

VITA AUCTORIS

NAME	Alexander G. Daniiov
BORN	Yugoslavia, 1939
EDUCATION	
Primary	Belgrade, Yugoslavia, 1946-1951
Secondary	Bicester, England, Grammar School, 1951-1953
	Bathurst, N.B., Canada, High School, 1954-1957
Universities	Sir George Williams University, 1959-1963, B.Sc.
	University of Ottawa, 1967 to present.